Journal of Thermal Biology 100 (2021) 103028

Contents lists available at ScienceDirect

Journal of Thermal Biology

journal homepage: www.elsevier.com/locate/jtherbio

Integrating thermal infrared stream temperature imagery and spatial stream network models to understand natural spatial thermal variability in streams

Matthew R. Fuller [a,*], Joseph L. Ebersole [b], Naomi E. Detenbeck [c], Rochelle Labiosa [d], Peter Leinenbach [e], Christian E. Torgersen [f]

[a] Oak Ridge Institute for Science and Education Postdoc at the U.S. EPA/ORD/CEMM Atlantic Coastal Environmental Sciences Division; 27 Tarzwell Drive, Narragansett, RI 02882, USA
[b] Research Fish Biologist at the U.S. EPA/ORD/CPHEA Pacific Ecological Systems Division; 200 Southwest 35th Street, Corvallis, OR 97333, USA
[c] Watershed and Estuarine Diagnostics Branch Ecologist at the U.S. EPA/ORD/CEMM Atlantic Coastal Environmental Sciences Division; 27 Tarzwell Drive, Narragansett, RI 02882, USA
[d] Water Quality Scientist at the U.S. EPA; 1200 Sixth Avenue, Seattle, WA 98101-3140, USA
[e] Aquatic and Landscape Ecologist at the U.S. EPA; 1200 Sixth Avenue, Seattle, WA 98101-3140, USA
[f] Supervisory Research Landscape Ecologist at the U.S. Geological Survey, Forest and Rangeland Ecosystem Science Center, Cascadia Field Station; University of Washington School of Environmental and Forest Sciences, Box 352100 Seattle, WA 98195, USA

ARTICLE INFO

Keywords:
Thermal regime
Middle Fork John Day River
Spatial autocorrelation
Airborne remote sensing
Cold-water habitat
Thermal infrared imagery
Spatial stream network model

ABSTRACT

Under a warmer future climate, thermal refuges could facilitate the persistence of species relying on cold-water habitat. Often these refuges are small and easily missed or smoothed out by averaging in models. Thermal infrared (TIR) imagery can provide empirical water surface temperatures that capture these features at a high spatial resolution (<1 m) and over tens of kilometers. Our study examined how TIR data could be used along with spatial stream network (SSN) models to characterize thermal regimes spatially in the Middle Fork John Day (MFJD) River mainstem (Oregon, USA). We characterized thermal variation in seven TIR longitudinal temperature profiles along the MFJD mainstem and compared them with SSN model predictions of stream temperature (for the same time periods as the TIR profiles). TIR profiles identified reaches of the MFJD mainstem with consistently cooler temperatures across years that were not consistently captured by the SSN prediction models. SSN predictions along the mainstem identified ~80% of the 1-km reach scale temperature warming or cooling trends observed in the TIR profiles. We assessed whether landscape features (e.g., tributary junctions, valley confinement, geomorphic reach classifications) could explain the fine-scale thermal heterogeneity in the TIR profiles (after accounting for the reach-scale temperature variability predicted by the SSN model) by fitting SSN models using the TIR profile observation points. Only the distance to the nearest upstream tributary was identified as a statistically significant landscape feature for explaining some of the thermal variability in the TIR profile data. When combined, TIR data and SSN models provide a data-rich evaluation of stream temperature captured in TIR imagery and a spatially extensive prediction of the network thermal diversity from the outlet to the headwaters.

1. Introduction

The thermal regime of aquatic environments can control ecosystem process rates (Demars et al., 2011), influence community composition (Caissie 2006), and provide an ecological resource (Magnuson et al., 1979). In freshwater environments, ecosystem processes such as respiration and organic matter decomposition rates are sensitive to temperature change, even more so than in terrestrial systems (Yvon-Durocher et al., 2012; Griffiths and Tiegs 2016). For individuals, water temperature can modify invertebrate emergence timing by altering development rates (Vannote and Sweeney 1980). At the community level, water temperature also drives annual rates of community

* Corresponding author.
E-mail address: fuller.matthew@epa.gov (M.R. Fuller).

https://doi.org/10.1016/j.jtherbio.2021.103028
Received 22 October 2020; Received in revised form 6 June 2021; Accepted 8 June 2021
Available online 12 June 2021

secondary production in streams (Patrick et al., 2019). Given the pervasive influence of temperature on freshwater ecosystems, characterizing thermal regimes is necessary to manage them.

There are many approaches for characterizing the temporal and spatial variability in a river network thermal regime (Caissie 2006; Webb et al., 2008; Steel et al., 2017; Isaak et al., 2020). At fine spatial resolutions, some fish species sensitive to temperature have been observed taking advantage of cold-water refuges <1 m^2 (Ebersole et al., 2001). At short temporal durations, some fish and freshwater mussels suffer from acute thermal stress when exposed to high temperatures for <1 h (Fowler et al., 2009; Payton et al., 2016) and may behaviorally thermoregulate in an attempt to avoid or reduce thermal stress (Dugdale et al., 2016; Corey et al., 2020; Wilbur et al., 2020). Over longer temporal durations, annual salmonid migrations require sufficiently distributed patches of cold-water habitat to reach their headwater spawning reaches (Isaak et al., 2018; Keefer et al., 2018). These migrations can take months to complete and occur during the warmest months of the year. To derive an appropriate river network thermal regime for a species, different types of data can be leveraged to capture the ecologically significant spatial and temporal variability of thermal habitats (Steel et al., 2017).

An ideal data set to evaluate river network thermal regimes includes two major components. First, the temperature data must cover the entire study area at a spatial resolution fine enough to capture the smallest river network features of interest (e.g., reaches or benthic habitat types across a network). Second, the temporal frequency must capture moments of significance to the species (i.e., spawning migrations, periods of chronic and acute thermal stress, or lethal exposure) (Steel et al., 2017). Airborne thermal infrared (TIR) remote sensing of rivers provides a fine spatial resolution thermal map for a river but may lack the temporal frequency necessary to capture moments of biological significance. In contrast, *in situ* temperature loggers provide high temporal frequency measurements but may not be able to identify small, but thermally significant, habitats across larger spatial extents or even within a river reach that is not fully mixed.

Airborne TIR imagery of rivers and streams has been collected with sensors mounted to helicopters and fixed-wing aircraft, but small unmanned aerial vehicles (UAVs) are emerging as a potential capture method as well (Dugdale et al., 2019). Thermal IR sensors collect fine resolution ($\sim$1 m or less pixel size) images of the stream surface when unobstructed by overhanging riparian structures. The thermal images can characterize a river's lateral and longitudinal temperature heterogeneity over a range of spatial scales from meters to tens of kilometers. Airborne TIR remote sensing has typically been conducted along mainstems (Fullerton et al., 2015) and larger tributaries in river networks (Dugdale et al., 2015). A potential limitation that affects airborne TIR imagery is that it only measures the "skin" or immediate surface temperature of the water (top 100 μm). This can affect the accuracy of TIR data if water velocity is very slow and the water column is thermally stratified (Torgersen et al., 2001). Despite recent increases in the availability of remotely sensed TIR data sets, there are benefits to leveraging them alongside more traditional *in situ* logger data to characterize river network thermal regimes. Methods for merging fine spatial resolution airborne TIR imagery with high temporal frequency *in situ* logger data are still being explored (Cristea and Burges 2009; Vatland et al., 2015; Dzara et al., 2019; Mejia et al., 2020). Distributed fiber-optic temperature sensing provides a combination of the high temporal frequency readings of *in situ* loggers, while also maintaining the finer spatial resolution of TIR, but lacks the extensive coverage of TIR (Selker et al., 2006).

When compared to airborne TIR data, *in situ* loggers provide a more thorough characterization of the temporal thermal variability at the reach scale in rivers but are less useful at characterizing the fine-scale spatial thermal heterogeneity across a river network. Using multiple *in situ* loggers deployed across a river network has been a productive approach to overcome the lack of spatial coverage for *in situ* loggers but is still unable to approach the 1-m spatial resolution that airborne TIR imagery provides. Instead, statistical models, such as spatial stream network (SSN) models (Peterson and Ver Hoef 2010) or generalized additive models, have been successful at using *in situ* logger data to make temperature predictions across large river network systems (Detenbeck et al., 2016; Isaak et al., 2017; Jackson et al., 2017). SSN model predictions are usually at coarser spatial resolutions (often 1-km reach scale) than airborne TIR imagery, but kriging interpolations and finer spatial resolution predictions are possible with denser arrays of *in situ* data (Ver Hoef et al., 2014).

SSN models are fit using temperature data from *in situ* loggers that can be deployed for any length of time if they appropriately characterize the desired focal period (e.g., annual, monthly, weekly, or daily temperature statistics). Consequently, these models can take advantage of data from multiple logger deployments from a diversity of collection agencies/institutions. Like other statistical models (e.g., Jackson et al., 2017), SSN models can use data from the mainstem as well as tributaries to predict temperature patterns across the entire river network. SSN models are uniquely designed to address and incorporate spatial autocorrelation associated with river network structure (dendritic branching) and the influence of downstream water flow (Peterson and Ver Hoef 2010; Ver Hoef and Peterson 2010). Explicitly including this spatial autocorrelation in SSN models generates predictions across the network that are often more accurate than other statistical models which do not address the spatial autocorrelation associated with dendritic structures or predominance of downstream flow (Frieden et al., 2014; Turschwell et al., 2016; Holthuijzen 2017). Additionally, SSN models include spatially explicit estimates of prediction error that provide a measure of uncertainty to compare prediction accuracy between tributaries with and without observation data. This network-wide characterization of river temperature allows SSN models to identify the cold-water habitat diversity within the mainstem (as airborne TIR imagery also provides) but also explore the heterogeneity of cold-water habitat in tributaries (Isaak et al., 2015). Because network-wide thermal heterogeneity is so vitally important for coldwater taxa ranging from stenothermal macroinvertebrates (Everall et al., 2015) to migratory salmon and trout (Frechette et al., 2018), accurately characterizing the thermal landscape of rivers is an important first step in understanding and managing thermal regimes for the protection of sensitive coldwater taxa.

The purpose of this study is to compare and then integrate TIR data, *in situ* temperature logger data, and SSN models to characterize thermal habitat of a river network and demonstrate the potential synergies and benefits of combining these different approaches. To address these project goals, airborne TIR imagery data (Table 1) and *in situ* data (Isaak et al., 2017) were obtained for the Middle Fork John Day (MFJD) River in Oregon, USA along with SSN models that predict the mean August daily maximum stream temperatures across the network (Fuller et al. Unpublished Results-a). We expected that because the SSN models are based on coarser scale predictors and observation spacing than the airborne TIR data, that the TIR data will exhibit finer scale longitudinal variability along the mainstem MFJD than the SSN model predictions. We also expect the finer scale thermal variation illustrated by the airborne TIR data to be explained by medium scale geomorphic, hydrologic, and hydrographic landscape features. To evaluate these expectations, first, previously developed SSN models (fit to *in situ* temperature logger data only) were used to predict the mean August maximum daily temperature across the MFJD River network to match the airborne TIR data collection dates. Second, the airborne TIR data and SSN model predictions were compared to see how well SSN model predictions characterize 1-km reach-scale temperature gradients (warming or cooling trends) along the mainstem of the MFJD. Third, SSN models were fit using observed TIR and *in situ* logger data to determine whether specific medium scale landscape features of the river network could help explain the fine spatial resolution thermal heterogeneity in the airborne TIR data that remained after accounting for the reach-scale temperature variation identified by SSN model predictions.

Table 1
TIR profile summary statistics for Middle Fork John Day River. Number of temperature observations represent the summary points derived for longitudinal temperatures from TIR imagery. The observation point was the median pixel temperature sampled from 5-13 pixels in the thalweg for each TIR image. Mean observation spacing is the average distance between these longitudinal temperature observations for each TIR flight. The profile starting river kilometer identifies where each TIR imagery data set began with river kilometer 0 designated at the outlet of the MFJD river and the higher river kilometer reaches moving upstream toward the headwaters. All raw TIR profile data are published in a USGS data release by Torgersen et al. (2021). See Table A1 for more details on TIR flights, specifications, and associated unpublished reports.

Date Collected (Year, Month, Day)	Profile length (km)	Number of temperature observations	Mean observation spacing (m)	Profile starting river km	Publications
1994 Aug 05	58.0	334	174	56.4	Torgersen et al. (1999) [a]; Torgersen et al., (2021)
1995 Aug 25	55.3	282	196	58.8	Poage et al. (1996) [a]; Torgersen et al., (2021)
1996 Aug 09	58.2	494	118	56.2	Torgersen et al. (2001) [b]; Torgersen et al., (2021)
1998 Aug 05	74.0	473	156	40.5	Torgersen et al., (2001); Fullerton et al., (2015); Torgersen et al. (2021)
2002 Aug 10	64.0	854	75	0.5	Torgersen et al. (2021)
2003 Aug 14	73.0	1,172	63	37.1	Torgersen et al. (2021)
2003 Aug 16	76.0	946	80	37.7	Fullerton et al., (2015); Torgersen et al., (2021)

[a] Subsets of TIR temperature observations (temperature metric = mean instead of median) from TIR flights in 1994 and 1995 were published in Poage et al. (1996) and Torgersen et al. (1999).
[b] Ground-truth data for the 1996 TIR flight were published in Torgersen et al. (2001).

2. Methods

2.1. Study area

The study area encompasses the Middle Fork John Day (MFJD) River in Oregon, USA (Fig. 1). The MFJD River is a major tributary to the John Day River which flows into the Columbia River mainstem roughly 300 km upstream from the Pacific Ocean. The MFJD basin area is approximately 2,050 km^2 with a mean annual discharge of 8 m^3/s. The river network has a total length of ~1,580 km according to the 1:100,000 scale flowline geometry of the National Hydrography Dataset Version 1 (United State Geological Survey (USGS), 2010). The elevation within the basin ranges between 600 m and 2,500 m above sea level and the mean annual precipitation varies from 300 mm to 1,300 mm. Mean annual air temperatures in the basin ranged from 4.4-9.1 °C with a mean of 6.4 °C between 1990 and 2015.

Migrating Pacific salmon use the headwaters of the MFJD River as spawning habitat, but many resident species (e.g., *Cottus* spp. and *Rhinichthys* spp.) are also present in the basin (Torgersen et al., 2006). The thermal regime of the MFJD River for these migrating salmonids approaches their thermal maximum and therefore they use cold-water habitats during their migration and holding period prior to spawning (Torgersen et al., 1999). Of the fish species in the system, several are designated as having "cool" or "cold" thermal habitat preferences (Zaroban et al., 1999).

2.2. Airborne thermal infrared (TIR) imagery

We used seven previously collected airborne TIR data sets from the years 1994, 1995, 1996, 1998, 2002, and two data sets from 2003 that covered parts of the mainstem MFJD River (Table 1, Torgersen et al., 2021). Six TIR data sets covered the upstream half of the MFJD mainstem between river km 50 and 110, while the 2002 profile starting at the outlet of the MFJD (confluence with North Fork John Day River) and spanned river km 1 through 64 (Table 1). All TIR data sets were collected in August with the intent of capturing the maximum August daily stream temperature. TIR imagery was processed and summarized into "temperature profiles" that extend longitudinally along the mainstem MFJD River (Tables 1 and A1, and Torgersen et al., 2021) and are composed of individual temperature observation points along the mainstem. For each captured TIR image, temperatures were recorded as the median value from 5-13 pixels sampled along the predominant flowline (Table 1). These points were approximately equally spaced within a given profile but that equal spacing ranged in length (50–200 m average spacing) across profiles (Table 1). Observation point temperatures were estimated similarly, but not identically among the seven profiles.

2.3. Spatial stream network models

Two different sets of spatial stream network (SSN) models were used in this study. The first set of SSN models were previously developed and used to predict the mean August daily maximum stream temperatures at the 1-km reach scale across the entire MFJD River network (Fuller et al. Unpublished Results-a). These were fit using only *in situ* temperature logger data and the predictions generated for the MFJD network were compared with the TIR profiles' observed data. The second set of SSN models were developed to test whether certain geomorphic and hydrologic features of the basin/network/channel were useful for explaining the fine resolution TIR data. This second set of SSN models were fit using a combination of TIR temperature observations and *in situ* logger data. We did not make any predictions using this second set of SSN models but used the SSN model as a statistical tool to test whether new geomorphic covariates we developed in this study could explain the fine spatial resolution TIR data. We will refer to the first set of SSN models described above as the "prediction SSN models" and the second set as the "TIR SSN models" hereafter.

2.3.1. Prediction SSN models

The prediction SSN models were built to predict the mean August daily maximum stream temperature using *in situ* temperature loggers (*n*

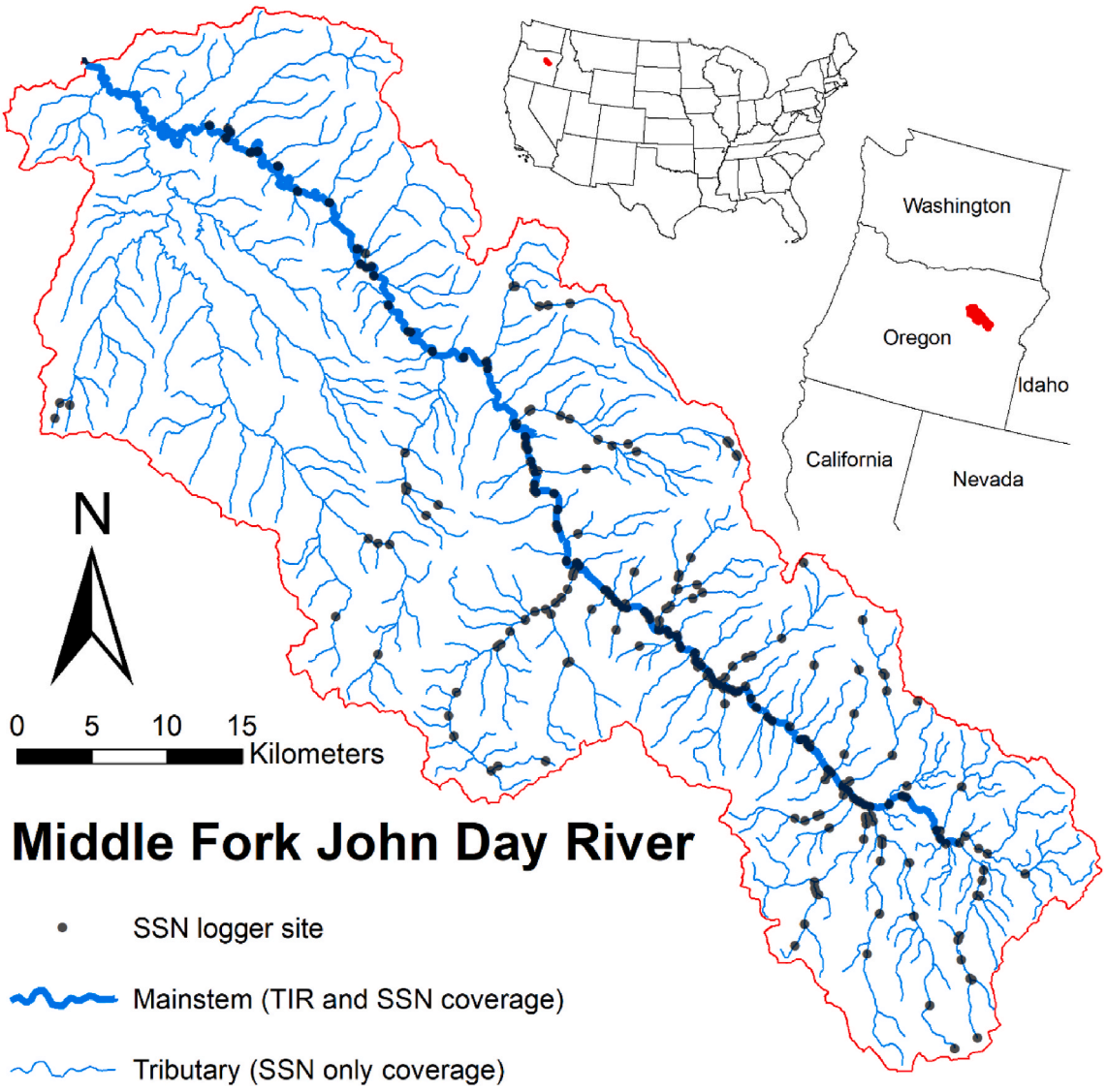

Fig. 1. Middle Fork John Day River study area highlighting the mainstem reach where thermal infrared imagery (TIR) was collected and the spatial stream network (SSN) *in situ* logger observation sites used to fit the prediction SSN model temperatures across the entire MFJD network.

= 206) that spanned the historic period of 1990–2015 with several covariates representing processes driven by the climate, water/land use, geology, and geography (Fuller et al. Unpublished Results-a, -b). These models represented a refinement of the original NorWeST SSN models that covered the MFJD basin (Isaak et al., 2017). A model selection process (Fuller et al. Unpublished Results-b) derived a suite of best fit models (n = 20) which were used with a model-averaging process (Burnham and Anderson 2002) to calculate the mean August daily maximum temperature predictions for ~1 km reaches across the MFJD River network for each of the corresponding TIR profile years (1994, 1995, 1996, 1998, 2002, and 2003). Interannual covariates included mean August air temperature (Dynamically Downscaled NCEP RegCM3 reanalysis model from Hostetler et al., [2011]) and mean August discharge (spatially explicit for each reach from Miller et al., [2018]). The SSN prediction models used only a linear with sill tail-up autocovariance structure. The hydrography network for the SSN model was based on the National Hydrography Data Version 1 and downloaded from the NorWeST SSN model database (Isaak et al., 2017).

2.3.2. TIR SSN models

TIR SSN models were fit to a combination of the observed TIR temperature data along with temperature observations from 85 *in situ* temperature loggers that had data collected concurrently with the TIR profiles. The *in situ* loggers were in tributaries and mainstem reaches and came from the NorWeST temperature database (Isaak et al., 2017). We extracted temperature records from *in situ* loggers that fell within the TIR flight times and chose the maximum temperature for each logger during the flight. In addition to the *in situ* temperature loggers, there were 4555 TIR observations from the seven TIR profiles. Individual TIR profiles ranged from 282-1172 independent temperature observations. Combining these two data sets makes a total of 4640 observation sites for the TIR SSN model fitting process.

Table 2
Geomorphic covariates and their descriptions for the TIR SSN model fits.

Covariate name	Units	Description
Observation temperature	degrees Celsius	Observed TIR or SSN *in situ* temperature logger temperature
SSN predicted temperature	degrees Celsius	Temperature predicted from prediction SSN models for the mean August daily maximum temperature
River Styles Geomorphic Classifications	NA	Classification of geomorphic features in the MFJD *sensu* O'Brien and Wheaton (2014). Rare classification types (classes with fewer than 10 instances) were grouped together as "Other" to avoid processing errors in Leave One Out Cross Validation procedures.
Entrenchment Ratio	unitless (m/m)	Ratio of bankfull channel width divided by the valley floor width transformed using the natural logarithm for normality
Entrenchment Ratio squared	unitless (m/m)	Ratio of bankfull channel width divided by the valley floor width transformed using the natural logarithm for normality squared
Entrenchment Ratio cubed	unitless (m/m)	Ratio of bankfull channel width divided by the valley floor width transformed using the natural logarithm for normality cubed
Distance to nearest spring	meters	Distance to the nearest spring location from the observation point
Nearest upstream tributary	meters	Upstream distance to the nearest tributary confluence
Nearest upstream tributary discharge ratio	unitless (cms/cms)	The discharge ratio of the nearest upstream tributary discharge divided by the discharge at the observation site. Discharge data obtained from the NHDPlus V2 Enhanced Runoff Method mean August discharge estimates.
reach sinuosity	unitless (km/km)	The sinuosity of a river reach calculated for ~1-km segments of river across the network using the ROCA tool (Bíl et al., 2018)
Valley end constriction	percent	A percent calculated from the width of a valley at the observation point divided by the maximum valley width measured within 500m upstream of the observation. Smaller percentages indicate the observation point may be located at the end of an unconfined valley where hyporheic and groundwater exchange are more likely to occur
End of Valley classification	NA	Boolean classification of observation sites as either at the end of an unconfined valley (where the valley narrows) or not. This designation uses a 15% or less threshold of the Valley End Constriction covariate to make the classification.

The purpose of our TIR SSN model fitting exercise was to try and explain the fine spatial heterogeneity of the TIR data that exists within the reach-scale predictions from the prediction SSN models. We fit our TIR SSN models using several hydrologic, hydrographic, and geomorphic covariates (hereafter discussed collectively as just "geomorphic" or "landscape" covariates/attributes) (Table 2). Covariates for the TIR SSN model fits included the predicted SSN model mean August daily maximum temperatures for the MFJD network (See section 2.3.1). Using the prediction SSN model output as a covariate in the TIR SSN models functions like a forward step-wise regression analysis where the covariates in the prediction SSN models are included prior to adding the new geomorphic covariates tested in this study. These temperature predictions provide a reach-scale estimate of temperature within which finer spatial resolution TIR observations vary. It is this residual fine-scale heterogeneity that we aim to explain using these new geomorphic covariates.

We included new geomorphic attributes hypothesized to influence thermal heterogeneity. For example, tributary confluences and valley morphology features have been associated with cold-water plumes that Chinook salmon prefer in the MFJD River (Torgersen et al., 1999). Hydrologic and hydrographic attributes included mean August discharge ratio of the nearest upstream tributary to that of the mainstem at their confluence (using discharge values from National Hydrography Dataset Plus Version 2 Enhanced Runoff Method – McKay et al., 2012), distance (m) to the nearest upstream tributary, and distance to the nearest spring (geospatial spring data from Brown et al., [2007, 2009; 2010]).

Our TIR SSN models used several landscape covariates to explain the observed fine resolution TIR temperature variability (Wondzell and Gooseff 2013a; Poole and Berman 2001; Dugdale et al., 2015). Geomorphic attribute covariates included: River Styles geomorphic reach classifications *sensu* O'Brien and Wheaton (2014), channel sinuosity (calculated for ~1 km reach segments using Bíl et al. (2018) ROCA tool), and an entrenchment ratio calculated from the bank full channel width divided by the valley floor width (along with its squared and cubed derivatives). The River Styles geomorphic classifications were designed to categorize the geomorphic restoration and recovery potential for each reach in the MFJD. These classifications, therefore, hold the spatially explicit geomorphological state of each reach in the network and can be used in the model to help predict which reaches have greater surface-subsurface water exchange.

Hyporheic exchange is expected to occur where the valley floor narrows at the downstream end of an unconfined reach, which usually results in cooler stream temperatures during the summer (Poole et al., 2008; Wondzell and Gooseff, 2013). Therefore, two covariates were developed to represent the proximity of sites to the end of an unconfined valley segment: 1) the valley floor width at a site as a percent of the maximum upstream valley floor width within 500 m upstream and 2) a binary variable indicating whether a site was located at the end of an unconfined valley when the percent of maximum upstream valley width was 15% or lower. Valley floor areas were delineated using the Valley Floor Mapper V1.0 (Kastens 2008) with a depth to flood of 15 cm above the bankfull depth and the National Hydrography Dataset Version 1 digital elevation model with a 30-m resolution (USGS, 2010). From these valley floor delineations, the valley floor width was measured by dividing the river network into 100-m reaches and measuring the width of the valley floor perpendicular to stream flow at the reach midpoint.

Twelve competing models were fit using these geomorphic and hydrologic covariates (Table 3). Each model included five core covariates intended to capture distinct processes. These included the prediction SSN mean August daily maximum temperatures, River Styles classifications, entrenchment ratio, distance to nearest spring, and channel sinuosity. Additional optional covariates included alternate versions of tributary and valley end covariates (distance to nearest upstream tributary and the tributary discharge ratio; and valley end constriction percent and end of valley classification, respectively). We supplemented models with the squared and cubed derivatives of the entrenchment ratio due to the quadratic results Dugdale et al. (2015) observed when predicting cold-water habitat locations with these higher power derivatives (Table 3).We used Akaike's Information Criterion (AIC) as a goodness of fit diagnostic statistic to compare among these models.

2.4. Analysis and comparison

All analyses were completed in the statistical software R v4.0 (R Core Team, 2020). Packages used during analysis and figure generation include: "ggridges" (Wilke 2020), "magrittr" (Bache and Wickham 2014), "patchwork" (Pedersen, 2019), "SNN" (Ver Hoef and Peterson 2010; Ver Hoef et al., 2014), "tidyverse" (Wickham 2017), and "trend" (Pohlert, 2020).

2.4.1. Mainstem profile spatial and temporal variability

We compared the distribution of temperatures collected in the TIR data with the predicted SSN temperature distributions for the MFJD mainstem. We treated the multiple TIR profiles as repeat observations of the MFJD River at its near maximum August temperature. The SSN predictions made for the same years were matched to these TIR profiles for a direct comparison between the empirical (TIR data) and theoretical

Table 3
SSN models fit using combinations of TIR and *in situ* logger observation data. Model formulae (fit01-12) include covariates as described in Table 2. A filled circle (●) identifies when a covariate was included in the model structure.

Covariate name	fit01	fit02	fit03	fit04	fit05	fit06	fit07	fit08	fit09	fit10	fit11	fit12
SSN predicted temperature	●	●	●	●	●	●	●	●	●	●	●	●
River Styles Geomorphic Classifications	●	●	●	●	●	●	●	●	●	●	●	●
reach sinuosity	●	●	●	●	●	●	●	●	●	●	●	●
Distance to nearest spring	●	●	●	●	●	●	●	●	●	●	●	●
Entrenchment Ratio	●	●	●	●	●	●	●	●	●	●	●	●
Entrenchment Ratio squared					●	●	●	●	●	●	●	●
Entrenchment Ratio cubed									●	●	●	●
Nearest upstream tributary	●		●		●		●		●		●	
Nearest upstream tributary discharge ratio		●		●		●		●		●		●
Valley end constriction			●	●			●	●			●	●
End of Valley classification	●	●			●	●			●	●		

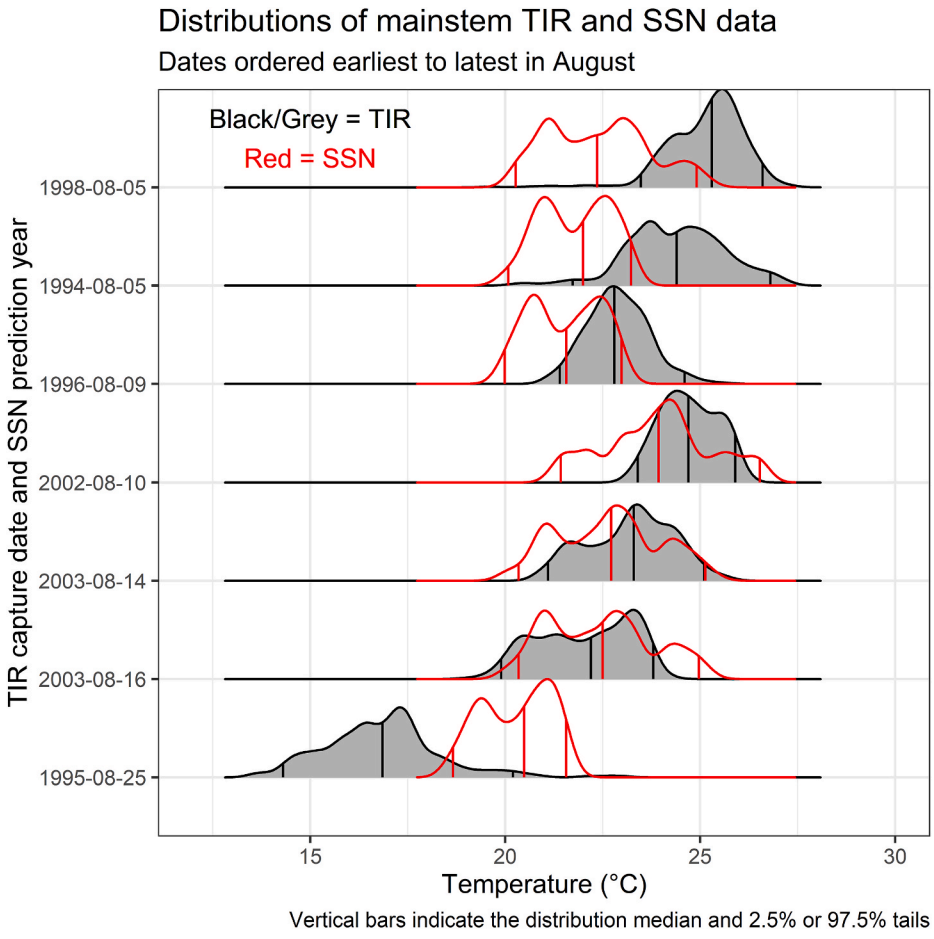

Fig. 2. Density distribution plots for each TIR profile (grey) and corresponding prediction SSN model predictions (red). Vertical lines for each distribution indicate the median value and delineate the 2.5% or 97.5% tails. Distributions are ordered by day of month in August.

(prediction SSN model output) characterization of temperature. Median values for these mainstem temperature distributions as well as the distribution range and modality for each profile determined how prediction SSN model output matched the TIR data measured in the field.

Qualitative comparisons were used to visually characterize each profiles' longitudinal pattern of downstream warming (*sensu* Fullerton et al., 2015) to determine if the predicted SSN temperature profiles matched the TIR data profiles for the MFJD mainstem. Additionally, the mainstem profiles were inspected for reach-scale thermal variability within 1-km reaches and for sections of the mainstem where consecutive 1-km reaches were generally cooler than others. These consecutive reaches with cooler temperatures were assessed temporally to see if they persist interannually among all profiles and between the TIR and SSN profiles. To delineate 1-km reaches for comparison, we used mainstem river kilometers starting at the MFJD outlet and measured river kilometers upstream.

2.4.2. *Reach temperature trends*

We leveraged the repeat observations from the multiple TIR profiles and their associated SSN prediction profiles to determine if individual mainstem river kilometer reaches tended to warm or cool in the downstream direction. We calculated the Sen's slope statistic (Sen 1968; Pohlert, 2020) for each mainstem river kilometer reach for each TIR profile. The Sen's slope statistic identifies a trend along a series and in this case, we used the distance along the reach to identify a trend in temperature. The mean Sen's slope value across all TIR profiles for a

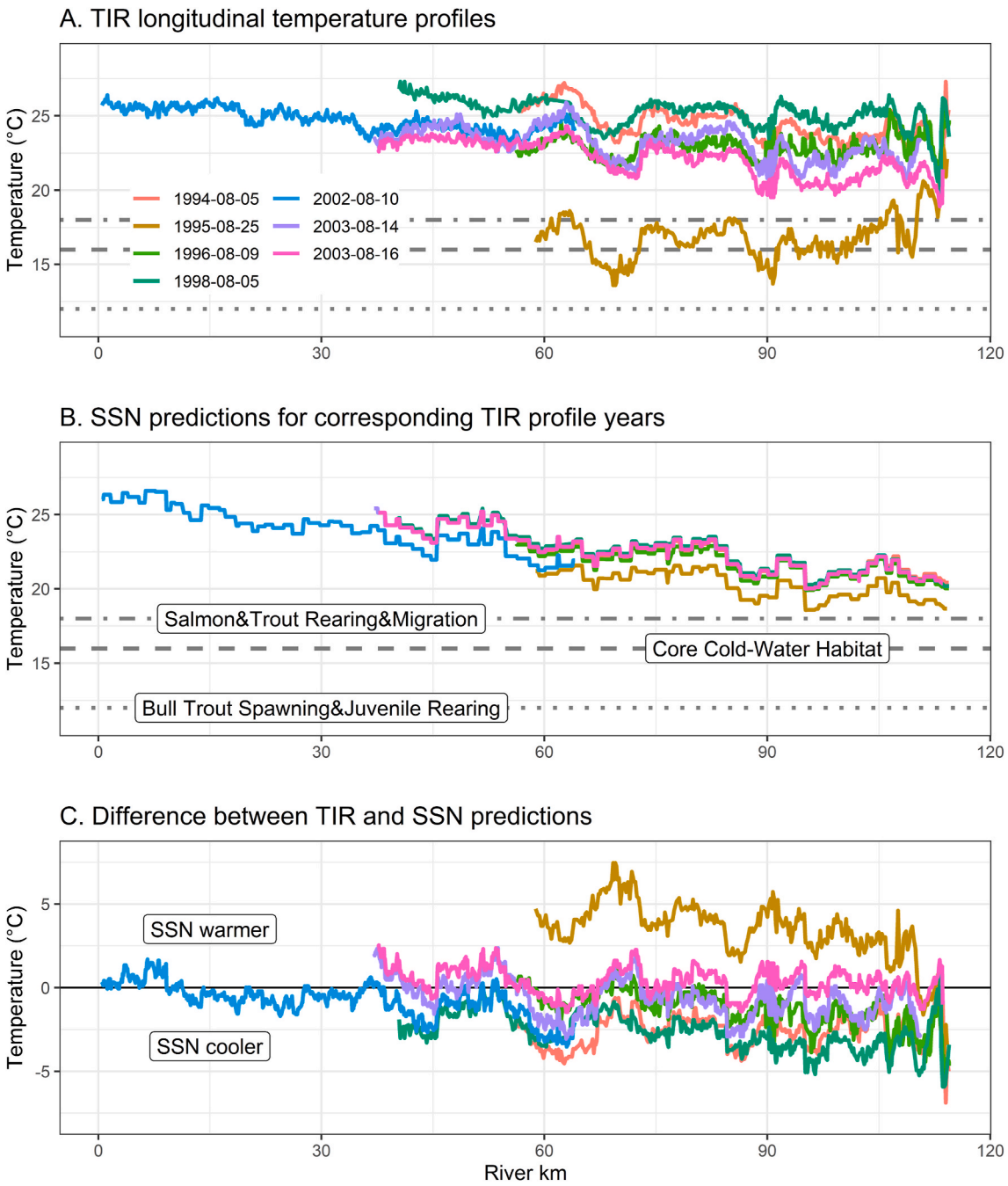

Fig. 3. Beginning at River km 0 (outlet) to 114 (headwaters) are the (A) observed TIR profiles, (B) prediction SSN model temperature profiles, and (C) difference between the two profiles along the mainstem of the MFJD. Horizontal lines in A and B indicate where Oregon State temperature water quality numeric criteria are for different fish species and habitat uses.

given reach was used to categorize each mainstem river kilometer reach with either a warming or cooing trend. If the mean Sen's slope statistic was negative, it was determined to be a warming reach because this represents temperature decreasing as the distance from the outlet increases (moving upstream). In contrast, a positive Sen's slope statistic indicated a cooling reach.

3. Results

3.1. Mainstem profile spatial and temporal variability

3.1.1. TIR and SSN mainstem profile characteristics

Individual TIR temperature profiles ranged from 5-10 °C depending on the year (Fig. 2). SSN mainstem predictions had similar temperature ranges, but their distribution medians were often cooler than the TIR profile distribution medians by as much as 7 °C. Raw TIR profile temperatures demonstrated both spatial and temporal variability along the mainstem (Fig. 3A). There was reach-scale (within river kilometers) spatial variability within profiles. However, there were stretches along the mainstem that were consistently cooler across years (e.g., lower temperatures surrounding river km 70 and 90). Across the entire mainstem, the TIR profiles followed a linear longitudinal trend (*sensu* Fullerton et al., 2015) with generally cooler temperatures in the headwaters and warmer temperatures toward the outlet (Fig. 3A), though reach-scale variability in temperatures was observed (i.e., various sequences of warming and cooling reaches). The 1995 TIR profile was an

exception to the downstream warming trend. The 1995 TIR profile was approximately 5–7 °C cooler than the other profiles and had slightly higher temperatures in the headwaters reaches than near the outlet. Among the other years, TIR profiles only varied, on average, by 3–4 °C.

The prediction SSN model predictions for each corresponding TIR profile had less reach-scale variability than the TIR profiles (Fig. 3B). However, cooler reaches in the prediction SSN profiles surrounding river km 90 matched those in the TIR profiles. The same lower temperatures observed near river km 70 in the TIR profiles were not apparent in the prediction SSN profiles (Fig. 3B). The prediction SSN profiles also did not exhibit as much interannual variability as the TIR profiles, but the 1995 SSN prediction was cooler than the others, which matched the cooler 1995 profile from the TIR data. Finally, the prediction SSN profiles also appeared to follow a longitudinal, linear, downstream, warming trend like the TIR profiles (Fig. 3B).

In situ logger data recorded concurrently with the TIR profiles indicate the TIR profiles were collected near the maximum daily temperature in August for most profiles (Appendix Fig. A2). TIR profile mean temperatures were warmer than the SSN model predictions except when collected later in August (1995 and 16 Aug 2003). The TIR profiles were 2–3 °C warmer than the SSN profiles which indicates the prediction SSN model generally underpredicted the maximum August daily temperature (Fig. 3C).

3.1.2. Reach temperature trends

The Sen's slope statistic calculated for warming and cooling trends had a larger range (−0.33 to 0.66) for TIR data than for the SSN predictions (−0.18 to 0.22) (Fig. 4). The magnitude of the Sen's slope statistic trends for the TIR data also were larger (0.049 ± 0.076 [mean absolute value ± SD]) than those calculated for the SSN prediction profiles (0.017 ± 0.037). This indicates the TIR profiles exhibit higher thermal heterogeneity within mainstem river kilometer reaches than the SSN models. Across the entire mainstem (river kilometers 0–120), the absolute magnitude of Sen's slope statistics was larger near the headwaters (river km 60–120) than in the lower reaches (river km 0–60) near the outlet (Fig. 4).

There was agreement on the temperature trend (warming or cooling) between the Sen's slope statistics for TIR data and SSN predictions in 81.7% of the mainstem river kilometer reaches (Fig. 5). In 8.7% of the mainstem river kilometer reaches, TIR profiles defined warming reaches while the SSN predictions indicated cooling. The remaining 9.6% of the mainstem river kilometer reaches had dissimilar trends with TIR trends cooling and SSN predictions warming. The mismatches in temperature trends were mostly restricted to the upper two-thirds of the mainstem (river km 35–120) but did not otherwise show any strong spatial bias or prevalence in one portion of mainstem. For many of the mismatched mainstem river kilometer reaches, the trends were very small (near zero Sen's slope statistic), especially between river kilometers 95 and 105.

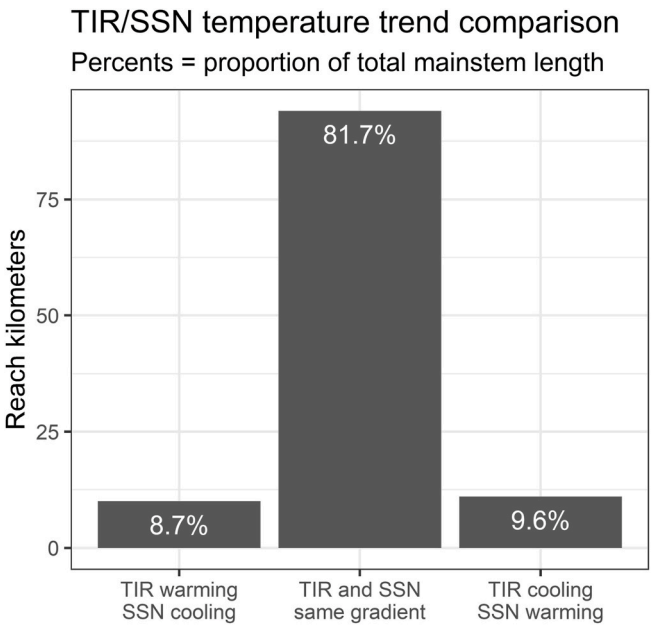

Fig. 5. Percent of trends that were similar or different between TIR and SSN data sources and the overall mainstem river length represented by matched or mismatched temperature trends.

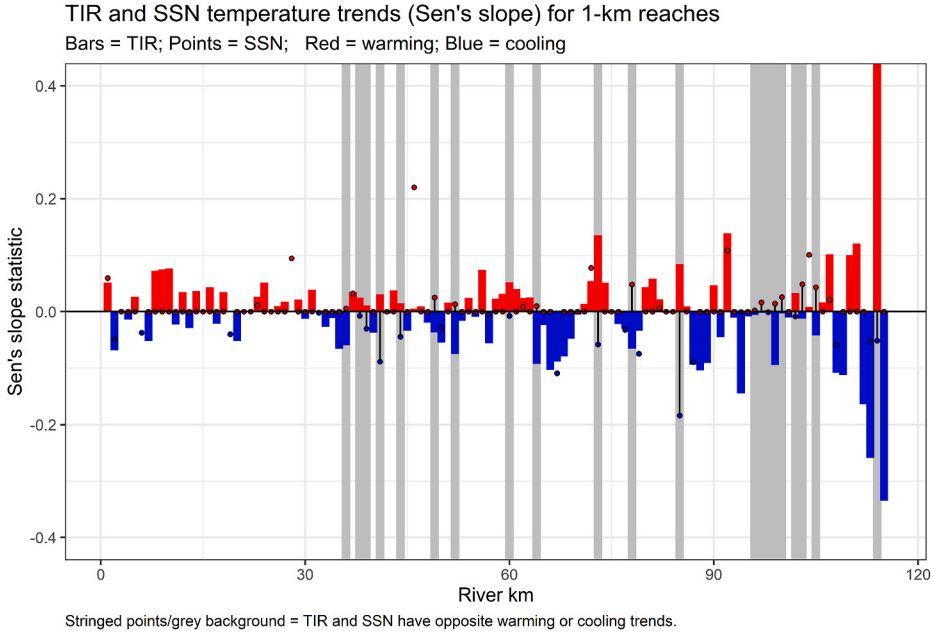

Fig. 4. Sen's slope statistic trends in temperature change for each 1 km reach along the MFJD mainstem. Bars represent TIR trends, while points represent SSN prediction trends. Positive Sen's slopes (red bars and points) indicate a warming trend, while negative (blue) indicates cooling trends. Tethered points within grey backgrounds indicate reaches where TIR and SSN prediction trends have opposing trend signs.

Table 4
TIR SSN model fit components of variance explained by the model and diagnostic statistics. Bold rows indicate models with similar fit to the observed data based on AIC values. Underlined row values indicates best model due to most parsimonious model structure and other diagnostic statistics (RMSPE and adjusted-R^2). Model ID formula structure as in Table 3.

	Variance Components					Model Statistics		
Model ID	Covariates	Tail-up	Tail-down	Euclidean	Nugget	AIC	RMSPE	Adj-R^2
fit01	0.259	0.499	0.003	0.132	0.109	19333.51	1.904	0.442
fit02	0.259	0.610	0.001	0.001	0.133	19354.98	1.903	0.443
fit03	**0.261**	**0.600**	**0.026**	**0.001**	**0.115**	**19326.37**	**1.899**	**0.445**
fit04	0.259	0.609	0.001	0.001	0.132	19354.96	1.904	0.443
fit05	0.261	0.529	0.028	0.045	0.139	19329.16	1.903	0.443
fit06	0.259	0.558	0.056	0.002	0.127	19355.35	1.903	0.443
fit07	0.261	0.613	0.001	0.008	0.120	19329.67	1.902	0.444
fit08	0.259	0.597	0.014	0.004	0.129	19357.58	1.904	0.442
fit09	**0.262**	**0.601**	**0.008**	**0.001**	**0.131**	**19326.24**	**1.901**	**0.444**
fit10	0.259	0.586	0.013	0.006	0.138	19351.79	1.906	0.441
fit11	0.261	0.623	0.001	0.002	0.117	19331.42	1.901	0.444
fit12	0.260	0.584	0.011	0.001	0.147	19351.86	1.904	0.442

Table 5
Coefficient estimate table for TIR SSN model fit03. Bold rows indicate statistically significant covariates and covariate abbreviations as in Table 2. River Styles classification acronyms: BC = bedrock-controlled; FP = floodplain; PC = planform-controlled.

Covariate	Raw Estimate	Raw Std. Error	Standardized Estimate	Standardized Std. Error	t-value	p-value
SSN prediction model temperatures	2.073	0.051	6.889	0.171	40.38	p « 0.0001
River Styles Class: BC Elongate Discontinuous FP	0.0000	NA	0.0000	NA	NA	NA
River Styles Class: Entrenched Bedrock Canyon	−0.508	0.595	−0.508	0.595	−0.85	0.39
River Styles Class: Low-Moderate PC Discontinuous FP	0.205	0.238	0.205	0.238	0.86	0.39
River Styles Class: Low-Moderate Sinuosity Gravel Bed	0.117	0.201	0.117	0.201	0.58	0.56
River Styles Class: Meandering Gravel Bed River	−0.748	0.918	−0.748	0.918	−0.81	0.42
River Styles Class: Meandering PC Discontinuous FP	0.431	0.555	0.431	0.555	0.78	0.44
River Styles Class: Rare Classification Group	0.580	0.358	0.580	0.358	1.62	0.11
Entrenchment ratio	−0.023	0.061	−0.049	0.133	−0.37	0.71
Distance to nearest spring (m)	−0.0003	0.0002	−0.414	0.245	−1.69	0.09
Distance to nearest upstream tributary (m)	**−0.0003**	**0.0001**	**−0.561**	**0.104**	**−5.39**	**p << 0.0001**
Sinuosity	−0.121	0.472	−0.031	0.122	−0.26	0.80
Valley end constriction	0.001	0.001	0.047	0.086	0.55	0.59

3.2. TIR SSN models

Two of the 12 competing TIR SSN models (fit03 and fit09 – Table 3) had nearly identical AIC values (19326.37 and 19326.24 respectively – Table 4) that were about 3 AIC units lower than the other models indicating their better fit to the observed data. The root mean squared prediction error (RMSPE) and adjusted-R^2 diagnostic statistics indicated fit03 had a slightly better fit to the data as well as being more parsimonious (Tables 4 and 3 respectively) and was selected as our best fit model. Fit03 included seven covariates of which two covariates (SSN predictions for mean August daily maximum temperature and the distance to the nearest upstream tributary) were statistically significant in the model (Table 5). The SSN mean August temperature covariate maintained the largest influence in the model based on its standardized coefficient estimate (Table 5).

4. Discussion

4.1. Temperature variation along mainstem

Prediction SSN model mainstem profiles had less interannual variability in stream temperature than the TIR profiles (Fig. 3A and B). This is likely because the SSN models predicted mean August maximum daily temperature rather than a single daily maximum temperature in August which is reflected in the TIR data. However, the SSN predictions for 1995 were cooler than the other years, which would indicate that in addition to the TIR data being collected later in the month, 1995 was also a cooler year. SSN models generally under predicted the maximum temperatures when compared to their respective TIR profiles (Fig. 3C). This was expected because the SSN predictions were made for the mean August daily maximum temperatures rather than maximum August temperature.

The TIR data were also more variable longitudinally than the predicted temperatures of the prediction SSN model (Fig. 3A versus 3B). Thus, the TIR data provided more information on potential acute temperature criteria exceedance and could also delineate the location and scale of thermal refuge areas better than SSN model predictions (Wawrzyniak et al., 2016). Furthermore, the TIR data also identified a cooler section of the mainstem (around river km 70) that the prediction SSN model did not. Around river km 70, the 2–3 °C drop in temperature observed in the TIR profiles was 1 °C or less in the prediction SSN model. This section of the mainstem flows through a valley meadow composed of alluvial sediment (O'Donnell 2012) and includes a number of relatively large (by volume) pools for the MFJD mainstem (Torgersen et al., 1999), which may be related to subsurface inputs that cool stream temperatures. Regardless of the mechanism driving these cooler stream temperatures, the SSN prediction model did not capture it.

4.2. Downstream temperature trends

The SSN and TIR data designated matching warming or cooling reaches across more than 80% of the mainstem of the MFJD. The ability of SSN models to predict temperature gradients that match TIR profile data for 80% of the mainstem has important management implications. Restoration managers working at scales >1 km with limited resources could leverage SSN models to identify warming reaches to reduce stream temperatures. TIR profile temperature trend magnitudes were larger than the trends from the prediction SSN model gradients for both

warming and cooling reaches. This is likely due to the much greater longitudinal variability observed in the TIR data. So, while SSN models can be useful first steps for locating coarse-scale warming reaches to restore, an empirical evaluation of those reaches using TIR imagery or another empirical method (e.g., distributed fiber-optic temperature sensing, or a dense array of *in situ* data loggers) is necessary to ensure important cold-water habitats are conserved at multiple spatial scales.

For the ~20% mismatched mainstem reach trends, we investigated whether the mismatches were more prevalent at transitions between warming and cooling reaches, but a chi-squared test did not find any evidence that these transition zones were where mismatches occurred. This suggests errors in spatial registration of TIR data points was not an issue. Furthermore, the mismatched trends (TIR warming and SSN cooling or vice versa) were equally abundant (9% or 10% respectively). Finally, there was a relatively equal prevalence of mismatches along the mainstem, suggesting that mismatches were not more common, for example, near the headwaters versus the outlet. However, there was a 10-km section of the mainstem, where the TIR and SSN gradients only matched for two of the ten 1-km reaches (Fig. 4). Although outside of the scope of these approaches, consideration of the heterogeneity and influence of surficial sediment geology (O'Sullivan et al., 2020), channel morphology (Dugdale et al., 2015), or floodplains (Singh et al., 2018) on hyporheic cooling (Faulkner et al., 2020) may be important areas of future consideration to enhance prediction in reaches where mismatches occur.

4.3. Explaining fine-scale spatial resolution TIR temperatures

Using TIR data in SSN models provided a statistical tool to try and resolve thermal variation in a dense observation data set along the mainstem portion of the river network. Our results, however, suggest that our choice of geomorphic covariates and methods for their development did not provide additional insight into potential geomorphic mechanisms controlling thermal variability in the longitudinal TIR profile data as we expected. Potential reasons for this result could include a mismatch in the spatial resolution of our geomorphic covariates or the variation within our covariates was not large enough to match and explain the TIR thermal diversity. In spatial statistical models, choosing or developing prediction covariates with similar (or finer) spatial resolution than the observed data maximizes the potential for a model to explain the variability in observed data (Turner et al., 2001). Geomorphic characteristics that can be derived from geospatial data sets that cover the entire study system are the most comprehensive way to easily generate covariates at similar spatial resolutions to the TIR data.

The geomorphology of a river network/basin (e.g., entrenchment ratio, valley constriction, and sinuosity) previously has been related to stream temperature (Dugdale et al., 2015), so the covariates we tested are reasonable explanatory variables. Sinuosity has been linked to hyporheic exchange at the reach scale (10–100 m), but our development of the sinuosity covariate used a larger ~1-km river segment to calculate sinuosity values which may have contributed to its inability to explain residual thermal variability in the TIR data observed at 60–200 m intervals (Table 1). In short, our sinuosity covariate spatial resolution may not have matched the TIR observation data and was unable to explain variation in the TIR data. Sinuosity derived at the 1-km reach scale was also statistically non-significant and unable to predict cold-water habitats in Canadian river basins (Dugdale et al., 2015).

SSN models are dependent on data sets that can adequately characterize the spatial autocorrelation among the observed data (stream temperature in this study). A recommended minimum number of observation sites for fitting SSN models is 50, but this can be reduced when all three forms of spatial autocorrelation (flow-connected/tail-up, flow-unconnected/tail-down, and Euclidean distance autocovariance structures) are not desired in the SSN model (Peterson and Ver Hoef 2010). The MFJD River system is a heavily sampled network, so we had 206 observation sites available to develop our prediction SSN models to compare with the TIR data. This relatively dense observation data (approximately one logger per 10 km of stream) contributed to the accuracy of the prediction SSN model that was able to predict warming and cooling reaches at the 1-km reach scale across 80% of the mainstem. This level of accuracy may not always be possible when SSN models are developed with fewer or less dense observation sites.

4.4. Combination of TIR data and SSN models

Thermal infrared data and SSN models complement each other in characterizing the thermal diversity of a river network. Each source of thermal information describes the river at a different spatial and temporal scale, but some overlap in their coverage along the mainstem of a river makes their combined use across the network valuable in a few ways. First, TIR data can inform SSN models and identify where they may be missing key explanatory covariates that are important for capturing spatial heterogeneity in stream temperatures. Second, comparing distributions of TIR profile temperatures with SSN model predictions quantifies the ability of SSN models to extend stream temperature predictions further into narrower and more heavily vegetated portions of the stream network. Third, for restoration activity planning, SSN models can help identify network reaches to focus resource-limited empirical efforts.

SSN models excel in their spatially extensive predictions of thermal heterogeneity across river networks which makes them a valuable complement to TIR data. If a network-wide accounting of available habitat based on temperature thresholds is necessary, SSN model predictions are an excellent tool. However, if the primary habitat evaluation is occurring along sections of a river where TIR data collection is possible, TIR data will provide more accurate longitudinal and two-dimensional information on thermal diversity along those corridors in the form of bank seeps or small tributary inputs that may be quite ecologically important to coldwater dependent taxa (Wilbur et al., 2020).

4.5. Management implications

As managers prepare for future climates, they will need to know where cold-water habitats exist in the landscape and how long they will persist (Morelli et al., 2020). TIR data and SSN models provide useful tools for determining the spatial distribution and heterogeneity of cold-water habitat. However, the temporal behavior of these cold-water habitats (when they exist and for how long) is just as important to properly managing species threatened with habitat loss due to climate warming. In one study, repeat TIR data collection found that only 39% of cold-water refuges could be relocated in surveys both within a season and between years (Dugdale et al., 2013). This suggests some cold-water habitat may not persist in space but appear sporadically when the correct conditions are met. In the future, known continuous cold-water habitats may shrink and split into patches that function as temporary steppingstones for movement across a system. This has already occurred along the mainstem Columbia River in the Pacific Northwest United States of America (Connor et al., 2019; Crozier et al., 2019; Keefer et al., 2018; Quinn and Adams 1996) and many smaller systems could follow a similar trajectory as cold-water habitats are restricted to headwater reaches from expected global warming (Almodóvar et al., 2012). Moving forward, understanding the temporal behaviors of these cold-water habitats will likely be necessary to manage species depending on cold-water habitat to complete their life cycle.

4.6. Limitations of study and future improvements

SSN models have been largely unable to predict patterns of daily temperature variability in part due to a lack of resolution in the covariates at that temporal scale, though SSN models can be fit to explain

daily metric variance when predictor data exist at the same timescale for a river network (Steel et al., 2016). This finer temporal resolution of SSN models could improve in the future as higher frequency spatial data sources and/or model outputs are generated to match the hourly/daily water temperature data resolution (Ficklin et al., 2012). Daily stream temperature models similar to SSN models have been fit to characterize large spatial extents and could provide alternatives to SSN models when this type of modeling product is necessary (Jackson et al., 2020). SSN models also generally have higher root mean square prediction error (RMSPE) when predicting maximum temperatures versus median or average monthly conditions (Detenbeck et al., 2016). This may help explain why our SSN model RMSPE values are higher than other SSN temperature models in the literature that focus on mean monthly temperatures instead of maximum statistics (Isaak et al., 2017).

We made a few assumptions when using the SSN prediction model temperatures as a predictor covariate in the TIR SSN model. First, the approach is similar to a forward step-wise regression analysis where the covariates for the prediction SSN model were being included first in the regression analysis and then subsequently followed up with the new geomorphic covariates we tested in this study. One limitation with this approach would be the potential for the new covariates to be highly correlated with those used in the prediction SSN model. To explore whether multicollinearity could potentially be the reason we saw few geomorphic covariates as statistically significant in our TIR SSN models, we looked at the correlations between all new geomorphic covariates in our TIR SSN models with those in the prediction SSN model. None of these correlations were >0.5 (or < -0.5), which suggests multicollinearity (generally problematic when correlations are < -0.7 or >0.7) among our model parameters was probably not why most were non-significant in the models (Appendix Fig. A4).

Another possible limitation to using the SSN predictions in the TIR SSN model is that interactions between the prediction SSN model covariates and the new geomorphic covariates are not tested during the model selection process. A few potential interaction terms supported in the literature include interactions between slope-, precipitation-, and discharge-related covariates from the prediction SSN models with the geomorphic feature classifications, entrenchment, and sinuosity covariates tested in the TIR SSN model (Wondzell, 2006; O'Sullivan et al., 2020). We fit new versions of our best TIR SSN model (fit03) with additional interaction terms to see whether these interactions were statistically significant in the models (Appendix Table A2). Several of these interaction terms were statistically significant in the updated model fits, but the original TIR SSN model geomorphic covariates did not shift in their statistical significance. This suggests our fit03 model may not be the best possible model to fit to the observed TIR data, but missing interaction terms did not result in the statistically non-significant terms in fit03.

Future analyses on the integration of TIR data and SSN models could look for study systems where digital elevation models are derived from lidar with 1-m spatial resolution or finer (O'Sullivan et al., 2020). These fine resolution digital elevation models can be used to derive geomorphic and channel morphology covariates that are spatially as refined as the 1-m resolution TIR imagery. This may improve the ability of derived geomorphic features for spatial models to predict the variability in TIR data and improve on the medium-scale geomorphic parameters used in this study.

5. Conclusions

The use of TIR data alongside SSN models can be a powerful approach for characterizing a river network thermal regime. While TIR data capture the fine spatial heterogeneity of temperatures along portions of the stream network visible to remote thermal imaging cameras, SSN models provide a spatially extensive prediction for thermal diversity across the entire network that includes heavily shaded headwater streams. TIR data provide model validation for how well SSN models characterize 1-km reach-scale patterns in temperature. While most of the geomorphic covariates we anticipated would explain the fine-resolution TIR data were statistically non-significant in our models, future exploration in this research area will continue to develop. Finer resolution topographic digital elevation models (1-m resolution) will become more readily available across larger landscapes to refine previously tested landscape covariates (O'Sullivan et al., 2020) and untested features of the landscape that were previously only possible through spatially continuous empirical habitat surveys (*sensu* Torgersen et al., 2006) could be derived. While spatial evaluation of cold-water habitats is important for locating these critical habitat patches as climate refuges, the temporal evaluation or permanence in the landscape will require additional scrutiny to determine their long-term effectiveness in protecting thermally sensitive species.

Funding

This work was supported by the United States Environmental Protection Agency Region 10 Regional Applied Research Effort Program through Interagency Agreements with the U.S. Forest Service (DW12924479) and Department of Energy (DW92429801-9, ORISE program).

CRediT authorship contribution statement

Matthew R. Fuller: Conceptualization, Methodology, Formal analysis, Software, Writing-Original Draft/Review & Editing, Visualization. **Joseph L. Ebersole:** Funding acquisition, Supervision, Conceptualization, Writing-Review & Editing. **Naomi E. Detenbeck:** Funding acquisition, Supervision, Formal analysis, Writing-Original Draft/Review & Editing. **Rochelle Labiosa:** Funding acquisition, Supervision, Conceptualization, Methodology, Writing-Review & Editing. **Peter Leinenbach:** Formal analysis, Writing-Original Draft/Review & Editing. **Christian E. Torgersen:** Data Curation, Validation, Writing-Review & Editing.

Acknowledgements

We acknowledge Nathan Poage, Russ Faux, Kathryn Ronnenberg, and Aimee Fullerton for their work on the thermal infrared profiles and associated metadata used in this study. Any use of trade, product, or firm names is for descriptive purposes only and does not imply endorsement by the U.S. Government.

APPENDIX

A. Airborne TIR imagery flight details

Table A1
Airborne thermal infrared imagery flight details along the Middle Fork John Day River mainstem. All raw TIR profile data are published in a United States Geological Survey data release by Torgersen et al. (2021).

Date (Year, Month, Day)	Flight time	Thermal infrared imager (make, model, wavelengths, type)	Sensor image size (pixels, W x H)	Viewing angle (degrees from nadir)	Meteoro-logical conditions	Speed of heli-copter (km/h)	Flight altitude above ground level (m)	Spatial resolu-tion (cm)	Image processing and calibration	Ground-truthing (sample size; mean absolute error ± standard error [°C])	Reference
1994 AUG 05	14:53–15:32	AGEMA Infrared Systems, Thermovision 800 FLIR, 8–12 μm (scanning array)	140 × 140	35–40	Cloudless; air temperature: 34 °C	40	250–300	20–60	Analog image data were calibrated for an emissivity of 0.96, corrected for atmospheric conditions (air temperature, relative humidity, and path length), converted to Celsius temperature, digitized, and stored in-flight at a rate of 3 frames/s on the hard drive of an onboard computer.	$n = 9$; 0.4 ± 0.1 SE	Methods and data in Torgersen et al. (1995) and Torgersen et al. (1999); ground-truthing data in Torgersen et al. (2001)
1995 AUG 25	13:40–14:20	AGEMA Infrared Systems, Thermovision 1000 FLIR, 8–12 μm (scanning array)	600 × 400	0	Cloudless but windy; air temperature: 18 °C	50	275–425	25–30	Analog image data were calibrated for an emissivity of 0.96, corrected for atmospheric conditions, converted to Celsius temperature, and recorded in-flight in S-Video format on Hi8 video tape. In the laboratory, video footage was transferred to S-VHS format, and image frames were captured with a TARGA + digitizing board and a DiaQuest video animation controller. In the captured grayscale thermal images, 256 shades of gray (0–255) corresponded linearly to the temperature range of 5–55 °C set during the flight.	$n = 3$; precise ground-truthing was not possible due to clock synchronization errors; comparisons between kinetic (in-stream) and radiant (image) temperature within a 15-min window indicated that mean absolute error was ~0.5 °C.	Methods and data in Poage et al. (1996)
1996 AUG 09	13:44–14:30	AGEMA Infrared Systems, Thermovision 1000 FLIR, 8–12 μm (scanning array)	600 × 400	0	Cloudless; air temperature: 37 °C	50	275–425	25–30	Same as in 1995.	$n = 13$; 0.5 ± 0.1 SE	Methods in Poage et al. (1996); ground-truthing data published in Torgersen et al. (2001)
1998 AUG 05	14:09–14:55	FLIR Systems, Thermovision 1000 FLIR, 8–12 μm (scanning array)	600 × 400	0	High scattered cirrus clouds; air temperature: 37 °C; relative humidity: 14%	50	300–450	30	Images were collected digitally and recorded directly from the sensor to an on-board computer at a rate of 1 frame/s. Radiant water temperatures were adjusted post-flight for the emissivity of water (0.96) and atmospheric conditions.	$n = 14$; 0.30 ± 0.05 SE	Methods and data in Torgersen et al. (2001) and Watershed Sciences (2003a)

(*continued on next page*)

Table A1 (*continued*)

Date (Year, Month, Day)	Flight time	Thermal infrared imager (make, model, wavelengths, type)	Sensor image size (pixels, W x H)	Viewing angle (degrees from nadir)	Meteoro-logical conditions	Speed of heli-copter (km/h)	Flight altitude above ground level (m)	Spatial resolu-tion (cm)	Image processing and calibration	Ground-truthing (sample size; mean absolute error ± standard error [°C])	Reference
2002 AUG 10	14:15–15:28	FLIR Systems, SC3000 LWIR, 8–9 μm (focal plane array)	320 × 240	0	Cloudless or high scattered cirrus clouds; air temperature: 31 °C; relative humidity: 13%	20–81	300–450	50	Same as in 1998.	$n = 4$; 0.28 ± 0.06 SE	Methods in Torgersen et al. (2001); methods and data in Watershed Sciences (2003b)
2003 AUG 14	13:57–15:30	FLIR Systems, SC3000 LWIR, 8–9 μm (focal plane array)	320 × 240	0	Cloudless; air temperature: 33 °C; relative humidity: 9%	28–106	300–490	54	Same as in 1998.	$n = 5$; 0.40 ± 0.05 SE	Methods in Torgersen et al. (2001); methods and data in Watershed Sciences (2004)
2003 AUG 16	13:48–15:08	FLIR Systems, SC3000 LWIR, 8–9 μm (focal plane array)	320 × 240	0	Cloudless; air temperature: 24 °C; relative humidity: 20%	35–109	300–490	54	Same as in 1998.	$n = 6$; 0.48 ± 0.05 SE	Methods in Torgersen et al. (2001); methods and data in Watershed Sciences (2004)

B. Prediction SSN model reach description

The prediction SSN model reaches (which can be spaced at ~1-km intervals) are not identical to the mainstem river kilometer reaches used to characterize reach-scale warming and cooling trends (Fig. A1). Prediction SSN model reaches are derived by delineating reaches at tributary confluences (Fig. A1A) and splitting segments that are more than 1 km (Fig. A1B) into approximately 1-km long reaches. Consequently, within each mainstem river kilometer reach, there is usually overlap from at least two SSN prediction reaches (Fig. A1C). To compare SSN predictions using the same warming/cooling trends, the SSN prediction reaches were sampled at each TIR observation point for the corresponding year that the TIR profile was collected (e.g., SSN predictions for 2002 were sampled at the 2002 TIR profile observation points). This sampling allowed the Sen's slope statistic trend calculations for each mainstem river kilometer reaches to be made for the prediction SSN model predictions and therefore spatially a direct comparison to the TIR Sen's slope statistic trends.

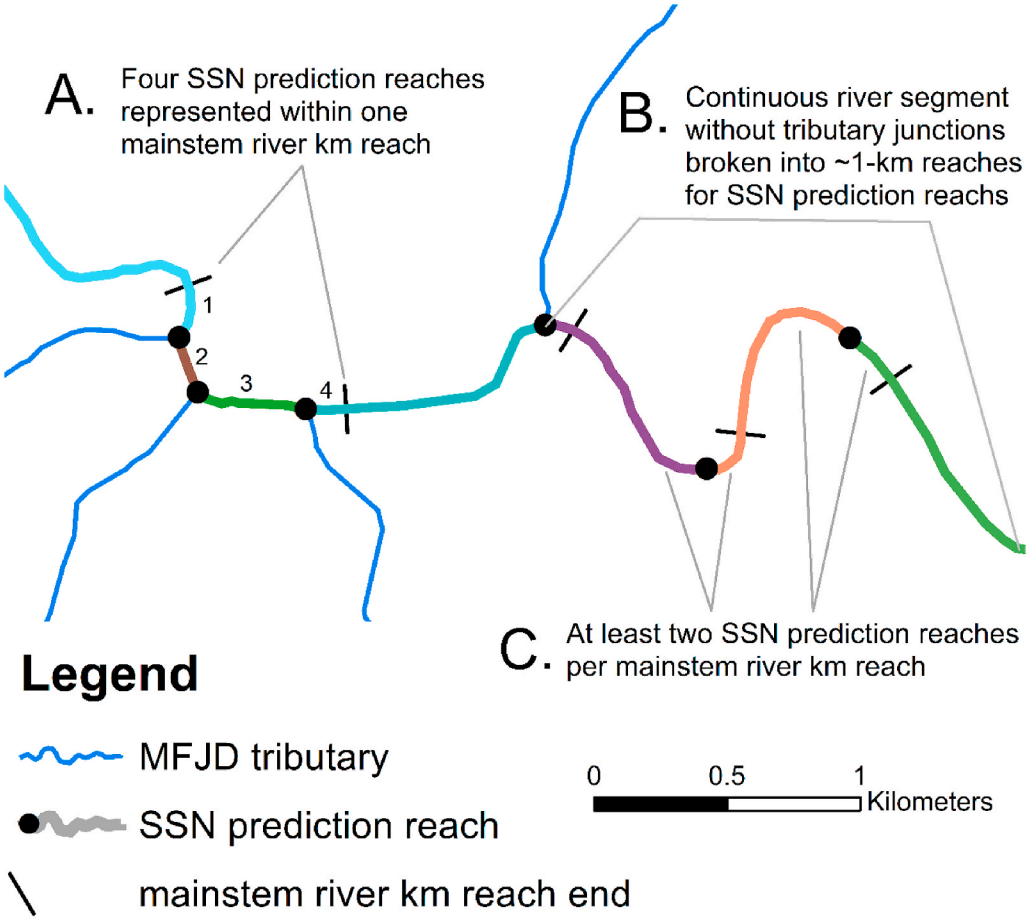

Fig. A1. Explanation of the overlap between the mainstem river kilometer reaches and prediction SSN model reaches along the mainstem MFJD. Prediction SSN model reaches are delineated by tributary confluences (part A dots) and at 1-km intervals when the reach does not have any tributary confluences (part B dots). The mainstem river kilometer reaches usually had at least two prediction SSN model reaches (part C) to evaluate temperature gradients within them but had more than two prediction SSN model prediction temperatures to evaluate temperature gradients when multiple tributaries join the mainstem river within an delineated mainstem river kilometer reach (part A).

C. Maximum daily temperatures

We used available *in situ* temperature logger data from deployments in the same years as the TIR profile flights to see how well TIR captured the maximum August temperature recorded across the network. The available *in situ* temperature records suggest the first half of August is warmer than the second (Appendix Figure A2). However, there was also variability in daily maximum temperatures across the month (likely due to weather) despite this average decline in temperature. Therefore, the timing of the TIR data collection appears sensitive to the collection date and provides one explanation for the cooler 1995 TIR profile which was collected on August 25.

In addition to the day of the month, the time of day is also important for TIR profile capture. The hour in which the maximum temperature was recorded at each of the 85 logger sites had a range of up to 7 h, though, most of the sites recorded maximum daily temperatures between 14:00 and 17:00 (Appendix Fig. A3), which overlaps the timeframes when TIR imagery was captured (Appendix Table A1). Similar collection timing sensitivity has also been observed in other TIR data evaluations (Vatland et al., 2015). The time lag between peak air temperature or solar radiation inputs and peak water temperature also varies with river discharge (Gu et al., 1998). These details demonstrate why it is important for TIR imagery metadata to

include precise details from the image capture methods and weather conditions. However, we also believe the snapshot TIR imagery provides in space could be grounded temporally if alternative data sources (e.g., *in situ* temperature loggers) are used for extended periods of time before and after TIR imagery collection. TIR imagery can also be useful pilot data for strategically placing *in situ* loggers in a system to characterize temporal thermal variability.

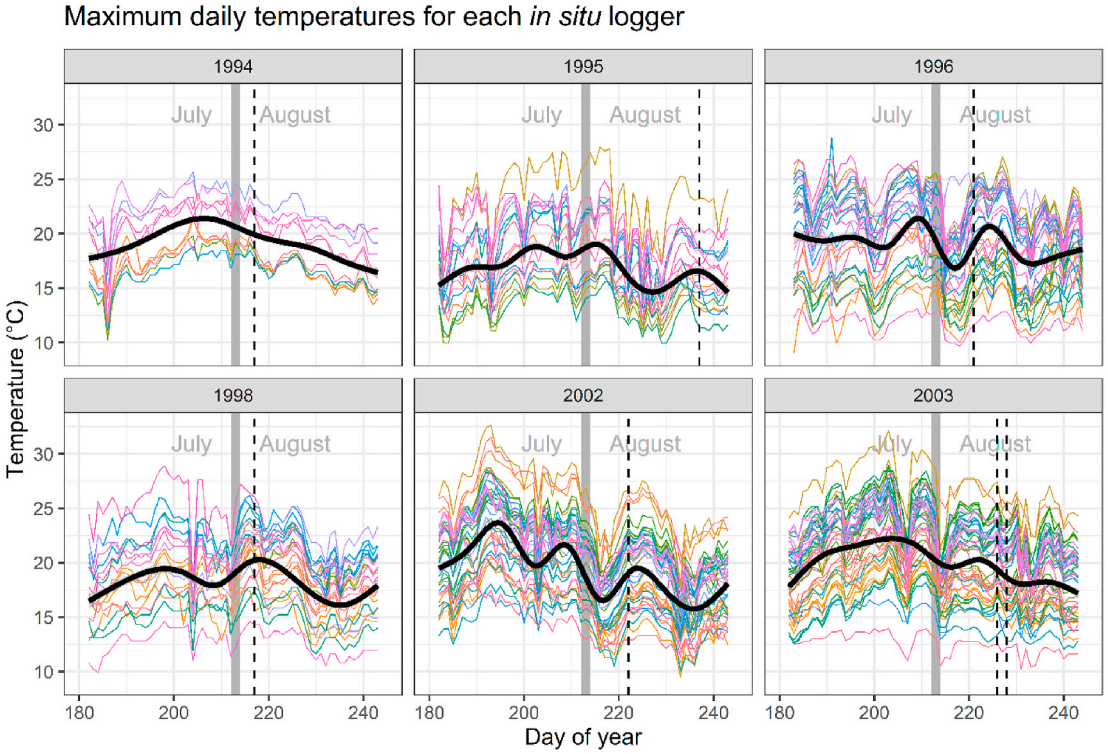

Fig. A2. *In situ* temperature logger maximum daily stream temperatures for same years as TIR data collection. Vertical dashed lines represent the day the TIR profiles were collected in each year. LOESS smoothing curve (bold-black) shows general trends in temperature across July and August (divided by grey vertical bar) for all sites (individual thin-colored lines) with complete data (i.e., all 31 days have temperature records).

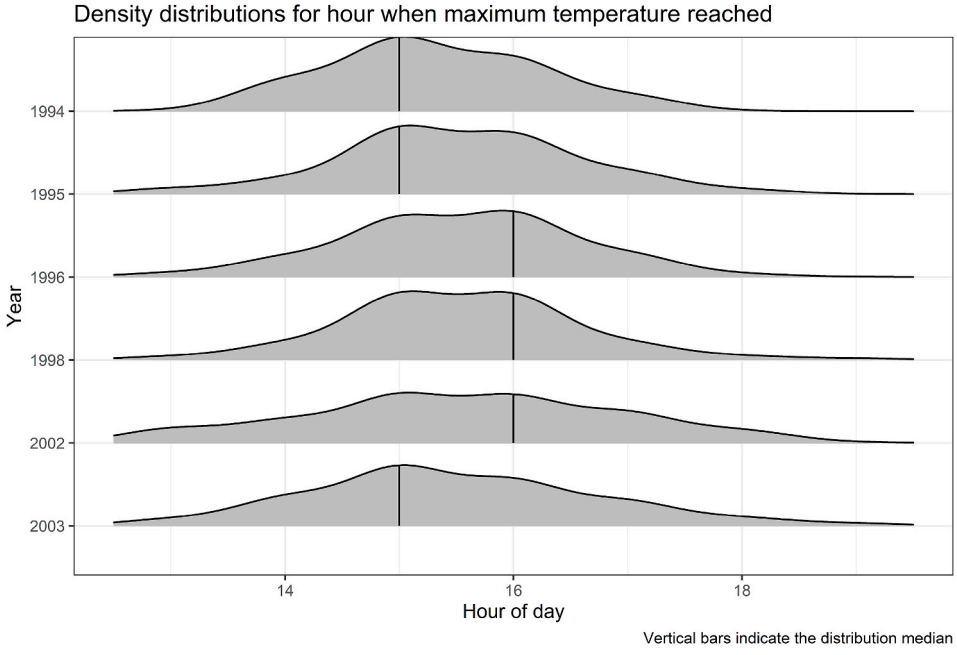

Fig. A3. Distributions for the hour of day when maximum stream temperature was recorded at each *in situ* observation logger site. Vertical lines are median values.

D. TIR SSN model vs Prediction SSN model covariates

We equated the inclusion of the mean August maximum daily temperatures as a predictor variable in the TIR SSN model as the equivalent of forcing all the prediction SSN model covariates into the TIR SSN model in a forward step-wise regression analysis. This initial inclusion of these covariates then

allowed us to test the other TIR SSN model covariates for their influence in explaining the remaining residual variation in the observed temperatures. Therefore, the TIR SSN model structures we tested are looking at the combinations of new geomorphic covariates after accounting for the prediction SSN model covariates.

One potential issue with this approach, is that there could be strong correlations between the new TIR SSN covariates and those included in the prediction SSN model. When there are strong correlations between covariates in a statistical model, multicollinearity can cause some covariates to be statistically non-significant predictors while their correlated parameter is highly significant. Multicollinearity effects usually manifest when correlations between parameters are larger than 0.7 (or < -0.7). Correlations between the TIR SSN and prediction SSN model covariates were all between -0.5 and 0.5 (Appendix Figure A4), which suggests that the reason the newly tested geomorphic covariates in the TIR SSN model were statistically non-significant is not due to multicollinearity between TIR SSN model and prediction SSN model covariates.

Combination of covariates in the model structure could also result in statistically non-significant covariates when continuous variables vary within categorical variables. For our best model fit (fit03), we included one categorical variable (River Styles Geomorphic Classifications) within which we see variation of our continuous variables. To address this potential issue, we fit two additional TIR SSN models using the best model fit (fit03) as the baseline model structure. The first model structure included just the categorical data and the SSN prediction temperatures as covariates (all continuous covariates were eliminated except for the prediction SSN model predicted temperatures from fit03 model structure). In contrast, the second model structure eliminated only the categorical covariate from fit03. These fits isolate whether the combination of categorical covariates and continuous covariates were interfering with each other in the models when determining the statistical significance of each covariates' coefficient. Our two additional model fits did not identify any new statistically significant covariates in either model when compared to the original fit03. Therefore, we do not believe the relationship between categorical and continuous covariates in the TIR SSN models contributed to why most geomorphic covariate coefficients were non-significant in our models.

A third potential issue with our model development process for the TIR SSN models is we could have missed important and potentially statistically significant interaction terms between the prediction SSN model covariates and those tested later in the TIR SSN models. We have identified a few interactions that are supported in the literature that could have been missed in our model selection process. These include interactions between slope and geomorphic classification covariates, slope and entrenchment covariates, precipitation and sinuosity covariates, and discharge and sinuosity covariates (Wondzell, 2006; O'Sullivan et al., 2020). We refit TIR SSN models that added these interaction terms to fit03 to see if including the interactions caused a change in the statistical significance of the original fit03 geomorphic covariates or if the interaction terms were statistically significant themselves (Appendix Table A2).

The interactions we tested were statistically significant in 3 of the 7 models, but only in one of the models did an original geomorphic covariate become significant (fit03I04 in Appendix Table A2). This model fit tested the inclusion of three interaction terms that varied by geomorphic classification from the River Styles system. What the statistically significant three-way interaction term between main channel slope, mean annual precipitation, and the River Styles geomorphic classifications suggests is that spatially cold-water habitats may not provide consistent refuges between wet and dry years. Generally, however, the inclusion of these new interactions terms (some statistically significant; some not) did not result in covariates originally in fit03 to become statistically significant.

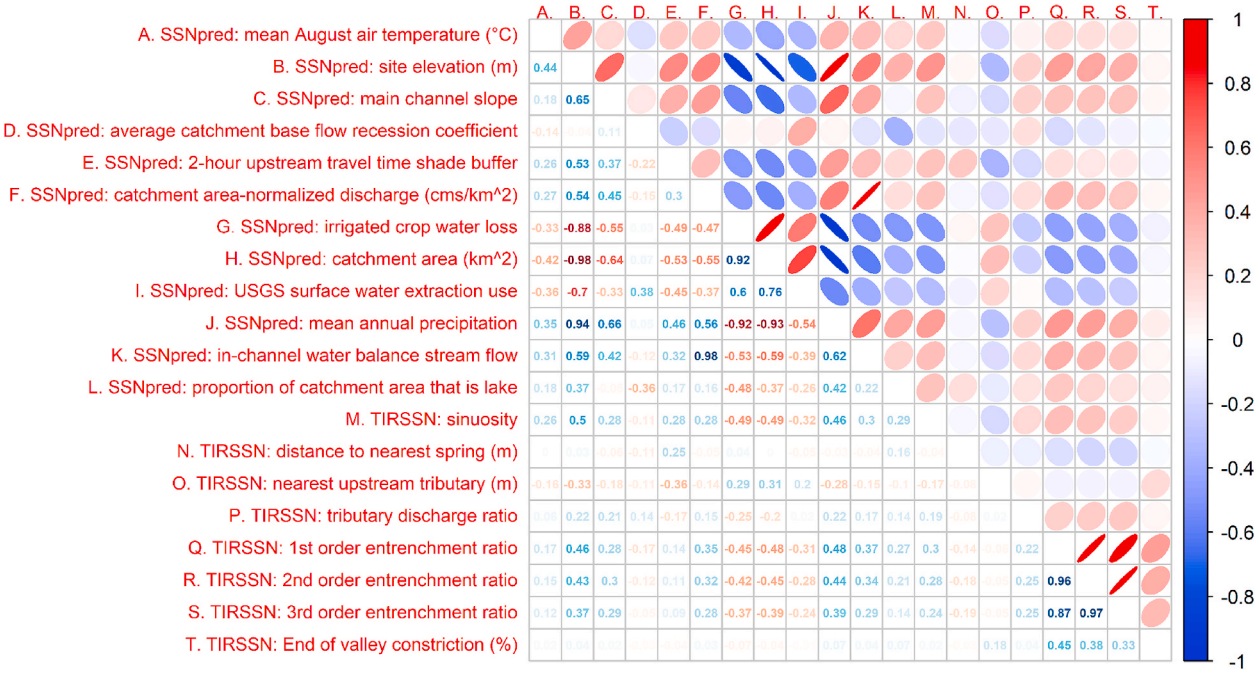

Fig. A4. Correlation plot for all TIR SSN model geomorphic covariates (prefix "TIRSSN:") and the SSN prediction model covariates (prefix "SSNpred:"). Color gradient represents direction of correlation value with cooler colors indicating negative correlations and warmer colors indicating positive correlations. Ellipses also indicate the direction and proportional strength of the correlation values. These correlations are for the 4640 combined TIR and *in situ* observation sites that were included in the TIR SSN model fits.

Table A2
Additional model structure TIR SSN model fits based off the best fit model (fit03) that explore additional interaction terms between the TIR SSN model and prediction SSN model covariates (Models fit03 I01–I07) and removing potential interactions between the categorical and continuous variables in the base fit03 model (fit03 C01, C02). Open circles represent statistically significant covariates included in the model fit while closed circles indicate non-significant covariates. Missing circles indicate that covariate was not used in the model fit.

Covariate name	fit03	fit03I01	fit03I02	fit03I03	fit03I04	fit03I05	fit03I06	fit03I07	fit03C01	fit03C02
TIR SSN MODEL COVARIATES										
SSN predicted temperature	○	○	○	○	○	○	○	○	○	○
River Styles Geomorphic Classifications	●	●	●	●	○	●	●	●	●	
reach sinuosity	●	●	●	●	●	●	●	●		●
Distance to nearest spring	●	●	●	●	●	●	●	●		●
Entrenchment Ratio	●	●	●	●	●	●	●	●		●
Entrenchment Ratio squared										
Entrenchment Ratio cubed										
Nearest upstream tributary	○	○	○	○	○	○	○	○		○
Nearest upstream tributary discharge ratio										
Valley end constriction	●	●	●	●	●	●	●	●		●
End of Valley classification										
INTERACTION TERMS TESTED										
Main channel slope x River Styles Geo. Class.		○			○					
Main channel slope x Entrenchment Ratio			○							
Mean annual precipitation x River Styles Geo. Class.				●	○					
Main channel slope x mean annual precipitation x River Styles Geo. Class. (three-way interaction term)					○					
Mean annual precipitation x reach sinuosity						●				
Area-normalized discharge x reach sinuosity							●			
In-channel water balance stream flow x reach sinuosity								●		

References

Almodóvar, A., Nicola, G.G., Ayllón, D., Elvira, B., 2012. Global warming threatens the persistence of Mediterranean brown trout. Global Change Biol. 18, 1549–1560. https://doi.org/10.1111/j.1365-2486.2011.02608.x.

Bache, S.M., Wickham, H., 2014. Magrittr: A Forward-Pipe Operator for R. R Package Version 1.5. https://CRAN.R-project.org/package=magrittr.

Bíl, M., Andrášik, R., Sedoník, J., Cícha, V., 2018. Roca – an ArcGIS toolbox for road alignment identification and horizontal curve radii computation. PloS One 13 (12), e0208407. https://doi.org/10.1371/journal.pone.0208407.

Brown, J., Wyers, A., Aldous, A., Bach, L., 2007. Groundwater and biodiversity conservation: a methods guide for integrating groundwater needs of ecosystems and species into conservation plans in the Pacific Northwest. The Nature Conservancy Report, 176pgs.

Brown, J., Wyers, A., Bach, L., Aldous, A., 2009. Groundwater-dependent biodiversity and associated threat: a statewide screening methodology and spatial assessment of Oregon. The Nature Conservancy Report. 79pgs.

Brown, J., Bach, L., Aldous, A., Wyers, A., DeGagné, J., 2010. Groundwater-dependent ecosystems in Oregon: an assessment of their distribution and associated threats. Front. Ecol. Environ. 9, 97–102. https://doi.org/10.1890/090108.

Burnham, K.P., Anderson, D.R., 2002. Model Selection and Multimodel Inference: A Practical Information–Theoretic Approach, second ed. Verlag, New York.

Caissie, D., 2006. The thermal regime of rivers: a review. Freshw. Biol. 51, 1389–1406.

Connor, W.P., Tiffan, K.F., Chandler, J.A., Rondorf, D.W., Arnsberg, B.D., Anderson, K.C., 2019. Upstream migration and spawning success of chinook salmon in a highly developed, seasonally warm river system. Reviews in Fisheries Science and Aquaculture 27, 1–50. https://doi.org/10.1080/23308249.2018.1477736.

Corey, E., Linnansaari, T., Dugdale, S.J., Bergeron, N., Gendron, J.F., Lapointe, M., Cunjak, R.A., 2020. Comparing the behavioral thermoregulation response to heat stress by Atlantic salmon parr (*Salmo Salar*) in two rivers. Ecol. Freshw. Fish 29, 50–62. https://doi.org/10.1111/eff.12487.

Cristea, N.C., Burges, S.J., 2009. Use of thermal infrared imagery to complement monitoring and modeling of spatial stream temperatures. J. Hydrol. Eng. 14, 1080–1090. https://doi.org/10.1061/(ASCE)HE.1943-5584.0000072.

Crozier, L.G., McClure, M.M., Beechie, T., Bograd, S.J., Boughton, D.A., Carr, M., Cooney, T.D., Dunham, J.B., Greene, C.M., Haltuch, M.A., Hazen, E.L., Holzer, D.M., Huff, D.D., Johnson, R.C., Jordan, C.E., Kaplan, I.C., Lindley, S.T., Mantua, N.J., Moyle, P.B., Myers, J.M., Nelson, M.W., Spence, B.C., Weitkamp, L.A., Williams, T. H., Willis-Norton, E., 2019. Climate vulnerability assessment for pacific salmon and steelhead in the California current large marine ecosystem. PloS One 14 (7), 1–49. https://doi.org/10.1371/journal.pone.0217711.

Demars, B., Manson, J., Olafsson, J., Gislason, G., Gudmundsdottir, R., Woodward, G., Reiss, J., Pichler, D., Rasmussen, J., Friberg, N, 2011. Temperature and the metabolic balance of streams. Freshw. Biol. 56 (6), 1106–1121. https://doi.org/10.1111/j.1365-2427.2010.02554.x.

Detenbeck, N.E., Morrison, A.C., Abele, R.W., Kopp, D.A., 2016. Spatial statistical network models for stream and river temperature in New England. U.S.A. Water Resources Research 52, 6018–6040.

Dugdale, S.J., Bergeron, N.E., St-Hilaire, A., 2013. Temporal variability of thermal refuges and water temperature patterns in an Atlantic salmon river. Rem. Sens. Environ. 136, 358–373.

Dugdale, S.J., Bergeron, N.E., St-Hilaire, A., 2015. Spatial distribution of thermal refuges analyzed in relation to riverscape hydromorphology using airborne thermal infrared imagery. Rem. Sens. Environ. 160, 43–55. https://doi.org/10.1016/j.rse.2014.12.021.

Dugdale, S.J., 2016. A practitioner's guide to thermal infrared remote sensing of rivers and streams: recent advances, precautions, and considerations. WIREs Water 3, 251–268. https://doi.org/10.1002/wat2.1135.

Dugdale, S.J., Franssen, J., Corey, E., Bergeron, N.E., Lapointe, M., Cunjak, R.A., 2016. Main stem movement of Atlantic salmon parr in response to high river temperature. Ecol. Freshw. Fish 25, 429–445. https://doi.org/10.1111/eff.12224.

Dugdale, S.J., Kelleher, C.A., Malcolm, I.A., Caldwell, S., Hannah, D.M., 2019. Assessing the potential of drone-based thermal infrared imagery for quantifying river temperature heterogeneity. Hydrol. Process. 33, 1152–1163. https://doi.org/10.1002/hyp.13395.

Dzara, J.R., Neilson, B.T., Null, S.E., 2019. Quantifying thermal refugia connectivity by combining temperature modeling, distributed temperature sensing, and thermal infrared imaging. Hydrol. Earth Syst. Sci. 23, 2965–2982. https://doi.org/10.5194/hess-23-2965-2019.

Ebersole, J.L., Liss, W.J., Frissell, C.A., 2001. Relationship between stream temperature, thermal refugia and rainbow trout *Oncorhynchus mykiss* abundance in arid-land streams in the northwestern United States. Ecol. Freshw. Fish 10 (1), 1–10. https://doi.org/10.1034/j.1600-0633.2001.100101.x.

Everall, N.C., Johnson, M.F., Wilby, R.L., Bennett, C.J., 2015. Detecting phenology change in the mayfly *Ephemera Danica*: responses to spatial and temporal water temperature variations. Ecol. Entomol. 40, 95–105. https://doi.org/10.1111/een.12164.

Faulkner, B.R., Brooks, J.R., Keenan, D.M., Forshay, K.J., 2020. Temperature decrease along hyporheic pathlines in a large river riparian zone. Ecohydrology 13, e2160. https://doi.org/10.1002/eco.2160.

Ficklin, D.L., Luo, Y., Stewart, I.T., Maurer, E.P., 2012. Development and application of a hydroclimatological stream temperature model within the Soil and Water Assessment Tool. Water Resour. Res. 48, W01511. https://doi.org/10.1029/2011WR011256.

Fowler, S.L., Hamilton, D., Currie, S., 2009. A comparison of the heat shock response in juvenile and adult trout (*Oncorhynchus mykiss*)—implications for increased thermal sensitivity with age. Can. J. Fish. Aquat. Sci. 66, 91–100. https://doi.org/10.1139/F08-192.

Frechette, D.M., Dugdale, S.J., Dodson, J.J., Bergeron, N.E., 2018. Understanding summertime thermal refuge use by adult Atlantic salmon using remote sensing, river temperature monitoring, and acoustic telemetry. Can. J. Fish. Aquat. Sci. 75, 1999–2010. https://doi.org/10.1139/cjfas-2017-0422.

Frieden, J.C., Peterson, E.E., Angus Webb, J., Negus, P.M., 2014. Improving the predictive power of spatial statistical models of stream macroinvertebrates using weighted autocovariance functions. Environ. Model. Software 60, 320–330. https://doi.org/10.1016/j.envsoft.2014.06.019.

Fuller, M.R., N. Detenbeck, P. Leinenbach, R. Labiosa, and D. Isaak. Unpublished Results-a. Implications for cold water stream temperature restoration from various management scenarios. In Preparation for Conservation Biology.

Fuller, M.R., N. Detenbeck, P. Leinenbach, R. Labiosa, and D. Isaak. Unpublished results-b. Spatial and temporal variability in thermal regime drivers for three drainage basins across the growing season. In Preparation for Journal of the American Water Resources Association.

Fullerton, A.H., Torgersen, C.E., Lawler, J.J., Faux, R.N., Steel, E.A., Beechie, T.J., Ebersole, J.L., Leibowitz, S.G., 2015. Rethinking the longitudinal stream temperature paradigm: region-wide comparison of thermal infrared imagery reveals unexpected complexity of river temperatures. Hydrol. Process. 29, 4719–4737.

Griffiths, N.A., Tiegs, S.D., 2016. Organic-matter decomposition along a temperature gradient in a forested headwater stream. Freshw. Sci. 35 (2), 518–533. https://doi.org/10.1086/685657.

Gu, R., Montgomery, S., Austin, T.A., 1998. Quantifying the effects of stream discharge on summer river temperature. Hydrol. Sci. J. 43, 885–904. https://doi.org/10.1080/02626669809492185.

Holthuijzen, M.F., 2017. A Comparison of Five Statistical Methods for Predicting Stream Temperature across Stream Networks. Utah State University M.S. Thesis. https://digitalcommons.usu.edu/etd/6535/.

Hostetler, S.W., Alder, J.R., Allan, A.M., 2011. Dynamically Downscaled Climate Simulations over North America: Methods, Evaluation and Supporting Documentation for Users: U.S. Geological Survey Open-File Report 2011-1238, p. 64.

Isaak, D.J., Young, M.K., Nagel, D.E., Horan, D.L., Groce, M.C., 2015. The cold-water climate shield: delineating refugia for preserving salmonid fishes through the 21st century. Global Change Biol. 21, 2540–2553. https://doi.org/10.1111/gcb.12879.

Isaak, D., Wenger, S., Peterson, E., Ver Hoef, J., Nagel, D., Luce, C., Hostetler, S., Dunham, J., Roper, B., Wollrab, S., Chandler, G., Horan, D., Parkes-Payne, S., 2017. The NorWeST summer stream temperature model and scenarios for the western U.S.: a crowd-sourced database and new geospatial tools foster a user community and predict broad climate warming of rivers and streams. Water Resour. Res. 53, 9181–9205.

Isaak, D.J., Luce, C.H., Horan, D.L., Chandler, G.L., Wollrab, S.P., Nagel, D.E., 2018. Global warming of salmon and trout rivers in the northwestern U.S.: road to ruin or path through purgatory? Trans. Am. Fish. Soc. 147, 566–587. https://doi.org/10.1002/tafs.10059.

Isaak, D.J., Luce, C.H., Horan, D.L., Chandler, G.L., Wollrab, S.P., Dubois, W.B., Nagel, D. E., 2020. Thermal regimes of perennial rivers and streams in the western United States. J. Am. Water Resour. Assoc. 56 (5), 842–867. https://doi.org/10.1111/1752-1688.12864.

Jackson, F.L., Fryer, R.J., Hannah, D.M., Malcolm, I.A., 2017. Can spatial statistical river temperature models be transferred between catchments? Hydrol. Earth Syst. Sci. 21, 4727–4745. https://doi.org/10.5194/hess-21-4727-2017.

Jackson, F.L., Fryer, R.J., Hannah, D.M., Malcolm, I.A., 2020. Predictions of national-scale river temperatures: a visualization of complex space–time dynamics. Hydrol. Process. 34, 2823–2825. https://doi.org/10.1002/hyp.13761.

Kastens, J.H., 2008. Some New Developments on Two Separate Topics: Statistical Cross Validation and Floodplain Mapping. PhD dissertation, University of Kansas, Ann Arbor. ProQuest/UMI. (Publication No. AAT 3316068.

Keefer, M.L., Clabough, T.S., Jepson, M.A., Johnson, E.L., Peery, C.A., Caudill, C.C., 2018. Thermal exposure of adult Chinook salmon and steelhead: diverse behavioral strategies in a large and warming river system. PloS One 13, 1–29. https://doi.org/10.1371/journal.pone.0204274.

Magnuson, J., Crowder, L., Medvick, P., 1979. Temperature as an ecological resource. Am. Zool. 19 (1), 331–343. https://doi.org/10.1093/icb/19.1.331.

McKay, L., Bondelid, T., Dewald, T., Johnston, J., Moore, R., Rea, A., 2012. National Hydrography Plus Version 2: User Guide.

Mejia, F., Torgersen, C., Berntsen, E., Maroney, J., Connor, J., Fullerton, A., Ebersole, J., Lorang, M., 2020. Longitudinal, later, vertical, and temporal thermal heterogeneity in a large impounded river: Implications for cold-water refuges. Remote Sens. 12 (9) https://doi.org/10.3390/RS12091386.

Miller, M.P., Carlisle, D.M., Wolock, D.M., Wieczorek, M., 2018. A database of natural monthly streamflow estimates from 1950 to 2015 for the conterminous United States. J. Am. Water Resour. Assoc. 54, 1258–1269. https://doi.org/10.1111/1752-1688.12685.

Morelli, T.L., Barrows, C.W., Ramirez, A.R., Cartwright, J.M., Ackerly, D.D., Eaves, T.D., Ebersole, J.L., Krawchuk, M.A., Letcher, B.H., Mahalovich, M.F., Meigs, G.W., Michalak, J.L., Millar, C.I., Quiñones, R.M., Stralberg, D., Thorne, J.H., 2020. Climate-change refugia: biodiversity in the slow lane. Front. Ecol. Environ. 18, 228–234. https://doi.org/10.1002/fee.2189.

O'Brien, G.O., Wheaton, J.M., 2014. River Styles® Report for the Middle Fork John Day Watershed, Oregon. Ecogeomorphology and Topographic Analysis Lab. Utah State University, Prepared for Eco Logical Research, and Bonneville Power Administration, Logan, Utah, p. 215.

O'Donnell, T., 2012. Evaluation of Stream Temperature Spatial Variation Using Distributed Temperature Sensing. Oregon State University. https://ir.library.oregonstate.edu/concern/graduate_thesis_or_dissertations/12579v193.

O'Sullivan, A.M., Devito, K.J., Ogilvie, J., Linnansaari, T., Pronk, T., Allard, S., Curry, R. A., 2020. Effects of topographic resolution and geologic setting on spatial statistical river temperature models. Water Resour. Res. 56 https://doi.org/10.1029/2020WR028122.

Patrick, C.J., McGarvey, D.J., Larson, J.H., Cross, W.F., Allen, D.C., Benke, A.C., Brey, T., Huryn, A.D., Jones, J., Murphy, C.A., Ruffing, C., Saffarinia, P., Whiles, M.R., Wallace, J.B., Woodward, G., 2019. Precipitation and temperature drive continental-scale patterns in stream invertebrate production. Science Advances 5, 1–10. https://doi.org/10.1126/sciadv.aav2348.

Payton, S.L., Johnson, P.D., Jenny, M.J., 2016. Comparative physiological, biochemical and molecular thermal stress response profiles for two unionid freshwater mussel species. J. Exp. Biol. 219, 3562–3574. https://doi.org/10.1242/jeb.140129.

Pedersen, T.L., 2019. Patchwork: the Composer of Plots. R Package Version 1.0.0. https://CRAN.R-project.org/package=patchwork.

Peterson, E., Ver Hoef, J., 2010. A mixed-model moving-average approach to geostatistical modeling in stream networks. Ecology 91 (3), 644–651.

Poage, N.J., Torgersen, C.E., Norton, D.J., Flood, M.A., 1996. Application of thermal infrared (TIR) and visible videography to the monitoring and restoration of salmonid habitat in the Pacific Northwest. In: Greer, J.D. (Ed.), 6th Forest Service Remote Sensing Applications Conference. American Society for Photogrammetry and Remote Sensing, Denver, CO, USA, pp. 376–379.

Pohlert, T., 2020. trend: Non-Parametric Trend Tests and Change-Point Detection. R package version 1.1.4. https://CRAN.R-project.org/package=trend.

Poole, G.C., Berman, C.H., 2001. An ecological perspective on in-stream temperature: natural heat dynamics and mechanisms of human-caused thermal degradation. Environ. Manag. 27, 787–802. https://doi.org/10.1007/s002670010188.

Poole, G., O'Daniel, S., Jones, K., Woessner, W., Bernhardt, E., Helton, A., Stanford, J., Boer, B., Beechie, T., 2008. Hydrologic spiraling: The role of multiple interactive flow paths in stream ecosystems. River Res. Appl. 24 (7), 1018–1031. https://doi.org/10.1002/rra.1099.

Quinn, T.P., Adams, D.J., 1996. Environmental changes affecting the migratory timing of American shad and sockeye salmon. Ecology 77 (4), 1151–1162. https://doi.org/10.2307/2265584.

R Core Team, 2020. R: A Language and Environment for Statistical Computing. R Foundation for Statistical Computing, Vienna, Austria. URL. https://www.R-project.org/.

Selker, J., Thévenaz, L., Huwald, H., Mallet, A., Luxemburg, W., van de Giessen, N., Stejskal, M., Zeman, J., Westhoff, M., Parlange, M., 2006. Distributed fiber-optic temperature sensing for hydrologic systems. Water Resour. Res. 42 (12), 1–8. https://doi.org/10.1029/2006WR005326.

Sen, P.K., 1968. Estimates of the regression coefficient based on Kendall's tau. J. Am. Stat. Assoc. 63 (324), 1379–1389. https://doi.org/10.2307/2285891.

Singh, H.V., Faulkner, B.R., Keeley, A.A., Freudenthal, J., Forshay, K.J., 2018. Floodplain restoration increases hyporheic flow in the Yakima River Watershed, Washington. Ecol. Eng. 116, 110–120. https://doi.org/10.1016/j.ecoleng.2018.02.001.

Steel, A.E., Sowder, C., Peterson, E.E., 2016. Spatial and temporal variation of water temperature regimes on the Snoqualmie River network. J. Am. Water Resour. Assoc. 52, 769–787. https://doi.org/10.1111/1752-1688.12423.

Steel, A.E., Beechie, T.J., Torgersen, C.E., Fullerton, A.H., 2017. Envisioning, quantifying, and managing thermal regimes on river networks. Bioscience 67 (6), 506–522. https://doi.org/10.1093/biosci/bix047.

Torgersen, C.E., Price, D.M., Li, H.W., McIntosh, B.A., 1995. Thermal refugia and chinook salmon habitat in Oregon: applications of airborne thermal videography. In: Mausel, P. (Ed.), Proceedings of the 15th Biennial Workshop on Color Photography and Videography. American Society for Photogrammetry and Remote Sensing, Terre Haute, pp. 167–171.

Torgersen, C.E., Price, D.M., Li, H.W., McIntosh, B.A., 1999. Multiscale thermal refugia and stream habitat associations of chinook salmon in Northeastern Oregon. Ecol. Appl. 9 (1), 301–319.

Torgersen, C.E., Faux, R.N., McIntosh, B.A., Poage, N.J., Norton, D.J., 2001. Airborne thermal remote sensing for water temperature assessment in rivers and streams. Rem. Sens. Environ. 76, 386–398.

Torgersen, C.E., Baxter, C.V., Li, H.W., McIntosh, B.A., 2006. Landscape influences on longitudinal patterns of river fishes: spatially continuous analysis of fish-habitat relationships. Am. Fish. Soc. Symp. 48, 473–492.

Torgersen, C.E., Fuller, M.R., Faux, R.N., Poage, N.J., Mejia, F.H., 2021. Airborne Thermal Infrared Remote Sensing of Summer Water Temperature in the Middle Fork John Day River (Oregon) in 1994-2003. U.S. Geological Survey data release. https://doi.org/10.5066/P9UQBZ2X.

Turner, M.G., Gardner, R.H., O'Neill, R.V., 2001. Landscape Ecology in Theory and Practice. Springer-Verlag, New York. https://doi.org/10.1007/b97434.

Turschwell, M.P., Peterson, E.E., Balcombe, S.R., Sheldon, F., 2016. To aggregate or not? Capturing the spatio-temporal complexity of the thermal regime. Ecol. Indicat. 67, 39–48. https://doi.org/10.1016/j.ecolind.2016.02.014.

United States Geological Survey (USGS), 2010. National Hydrography Dataset (Version USGS National Hydrography Dataset Plus Version 1 (NHDPlusV1) for Hydrologic Region 17 (Pacific Northwest). URL. https://nhdplus.com/NHDPlus/NHDPlusV1_17.php.

Vannote, R.L., Sweeney, B.W., 1980. Geographic analysis of thermal equilibria: a conceptual model for evaluating the effect of natural and modified thermal regimes on aquatic insect communities. Am. Nat. 115, 667–695. https://doi.org/10.1086/283591.

Vatland, S.J., Gresswell, R.E., Poole, G.C., 2015. Quantifying stream thermal regimes at multiple scales: combining thermal infrared imagery and stationary stream temperature data in a novel modeling framework. Water Resour. Res. 51, 31–46.

Ver Hoef, J.M., Peterson, E.E., 2010. A moving average approach for spatial statistical models of stream networks (with discussion). J. Am. Stat. Assoc. 105, 6–18. https://doi.org/10.1198/jasa.2009.ap08248.

Ver Hoef, J.M., Peterson, E.E., Clifford, D., Shah, R., 2014. SSN: an R package for spatial statistical modeling on stream networks. J. Stat. Software 56 (3), 1–43. URL. http://www.jstatsoft.org/v56/i03/.

Watershed Sciences, 2003a. Description of Aerial Surveys in the Upper John Day River Basin: Thermal Infrared and Color videography. Surveys of the Middle Fork John Day River and North Fork John Day River conducted in 1998 for the Oregon Department of Environmental Quality. Unpublished report Corvallis, Oregon.

Watershed Sciences, 2003b. Aerial Surveys in the John Day River Basin: Thermal Infrared and Color Videography. Surveys of the Middle Fork John Day River and North Fork John Day River Conducted in 2002 for the Oregon Department of Environmental Quality. Unpublished Report. Corvallis, Oregon.
Watershed Sciences, 2004. Aerial Surveys in the John Day River Basin: Thermal Infrared and Color videography. Surveys of the Middle Fork John Day River, South Fork John Day River, Clear Cr., and Camp Cr. Conducted in 2003 for the Dept. Of Fisheries and Wildlife (Oregon State University) and the U.S. Bureau of Reclamation. Unpublished report, Corvallis, Oregon.
Wawrzyniak, V., Piégay, H., Allemand, P., Vaudor, L., Goma, R., Grandjean, P., 2016. Effects of geomorphology and groundwater level on the spatio-temporal variability of riverine cold water patches assessed using thermal infrared (TIR) remote sensing. Rem. Sens. Environ. 175, 337–348. https://doi.org/10.1016/j.rse.2015.12.050.
Webb, B.W., Hannah, D.M., Moore, R.D., Brown, L.E., Nobilis, F., 2008. Recent advances in river and stream temperature. Hydrol. Process. 22, 902–918.
Wickham, H., 2017. Tidyverse: Easily Install and Load the 'Tidyverse'. R Package version 1.2.1. https://CRAN.R-project.org/package=tidyverse.
Wilbur, N.M., O'Sullivan, A.M., MacQuarrie, K.T.B., Linnansaari, T., Curry, R.A., 2020. Characterizing physical habitat preferences and thermal refuge occupancy of brook trout (*Salvelinus Fontinalis*) and Atlantic salmon (*Salmo Salar*) at high river temperatures. River Res. Appl. 36, 769–783. https://doi.org/10.1002/rra.3570.
Wilke, C.O., 2020. Ggridges: Ridgeline Plots in 'ggplot2'. R Package version 0.5.2. https://CRAN.R-project.org/package=ggridges.
Wondzell, S., 2006. Effect of morphology and discharge on hyporheic exchange flows in two small streams in the Cascade Mountains of Oregon, USA. Hydrol. Process. 20, 267–287. https://doi.org/10.1002/hyp.5902.
Wondzell, S., Gooseff, M., 2013. Geomorphic controls on hyporheic exchange across scales: watersheds to particles. Treatise on Geomorphology, 9. Academic Press, San Diego, CA, pp. 203–218.
Yvon-Durocher, G., Caffrey, J.M., Cescatti, A., Dossena, M., Del Giorgio, P., Gasol, J.M., Montoya, J.M., Pumpanen, J., Staehr, P.A., Trimmer, M., Woodward, G., Allen, A.P., 2012. Reconciling the temperature dependence of respiration across timescales and ecosystem types. Nature 487, 472–476. https://doi.org/10.1038/nature11205.
Zaroban, D.W., Mulvey, M.P., Maret, T.R., Hughes, R.M., Merritt, G.D., 1999. Classification of species attributes for pacific northwest freshwater fishes. Northwest Sci. 73, 81–93.

Matthew Fuller is an Oak Ridge Institute for Science and Education postdoctoral research scientist with the United States Environmental Protection Agency. He received his PhD from Duke University while studying freshwater organism landscape genomics. Dr. Fuller has conducted freshwater research in a variety of fields including ecology, geomorphology, and biogeochemistry. His interests (currently) lean toward understanding the ecology of aquatic species while working at the landscape-unit scale within freshwater river networks.

Joe Ebersole is a Research Fisheries Biologist with the US EPA's Pacific Ecological Systems Division where he conducts research on freshwater fish, habitat, and water quality. A particular emphasis of Dr. Ebersole's research has been on water temperature effects on fish behavior, growth, and survival. His current research is examining the resilience and recovery potential of streams and rivers challenged by extreme events like wildfires, droughts, and floods.

Dr. Naomi Detenbeck is a watershed ecologist working at the US EPA Atlantic Coastal Environmental Sciences Division in Narragansett, RI, with over 30 years of experience in studying a broad array of aquatic systems (lakes, streams, wetlands, estuaries). Her recent work focuses on development of decision support tools (Watershed Management Optimization Support Tool) and virtual data portals for estuarine data discovery, access, and visualization (Estuary Data Mapper). She has recently published spatial statistical models describing thermal and flow regimes for the New England region, and is working on methods to refine spatial statistical network models.

Rochelle Labiosa is a Physical Scientist in the Water Division of EPA's Region 10 Office in Seattle WA. Dr. Labiosa is located in the Water Quality Standards Program and supports the scientific and policy development and implementation of water quality standards, which describe the desired condition of a water body and the means by which that condition will be protected or achieved, for state and tribal programs in Region 10 (Alaska, Idaho, Oregon, and Washington).

Peter Leinenbach is an Aquatic Ecologist at the United States Environmental Protection Agency in the Seattle regional office since 1996. Peter has worked primarily on technical assessment and modeling support for Clean Water Act TMDL projects, and GIS landscape analysis and support for the USEPA National Surveys.

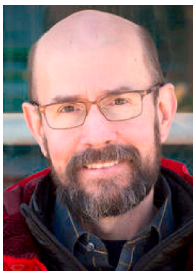

Christian Torgersen is a research landscape ecologist in the U.S. Geological Survey, Forest and Rangeland Ecosystem Science Center, Cascadia Field Station located in the School of Environmental and Forest Sciences at the University of Washington in Seattle, WA. Dr. Torgersen conducts research on quantifying and explaining spatial heterogeneity in aquatic and terrestrial ecosystems and identifying how scale of observation influences our understanding of ecological patterns and processes.